SOUTHWEST RESEARCH INSTITUTE®

Mechanical and Materials Engineering Division
March 29, 2007

VIA FEDEX

Mr. Matthew Quinney
Department of the Interior
Minerals Management Service
Procurement Operations Branch
MS2500, 381 Elden Street
Herndon, VA 20170

Subject: Southwest Research Institute (SwRI®) Project 18.12210
             Minerals Management Service (MMS) Order No. 0106PO39569
             "Synthetic-Based Drilling Fluid Droplet Study" – Final Report

Dear Mr. Quinney:

In accordance with the provisions of the above-noted Order, please find enclosed five copies of the Final Report, along with five CDs containing both Word and PDF versions of the report.

It has been a pleasure working with you on this project, and we look forward to our future endeavors.

If you have any questions, please feel free to contact me at 210-522-2350 or rhart@swri.org.

Sincerely,   APPROVED

Robert A. Hart   J. Christopher Buckingham
Senior Research Engineer   Manager, Multiphase Flow

RAH:*tw*

Enclosures

c: Olivia F. Adrian, MMS
      R. L. Bass, SwRI
      D. M. Deffenbaugh, SwRI
      R. Rodriguez, SwRI
      Record Copy B

FALL VELOCITY OF SYNTHETIC-BASED DRILLING FLUIDS IN SEAWATER

FINAL REPORT

SwRI® Project No. 18.12210
MMS Order No. 0106PO39569

Prepared for:

Minerals Management Service
361 Elden Street
Herndon, VA 20170

March 2007

S O U T H W E S T   R E S E A R C H   I N S T I T U T E®

S A N   A N T O N I O   H O U S T O N
D E T R O I T   W A S H I N G T O N ,   D C

FALL VELOCITY OF SYNTHETIC-BASED DRILLING FLUIDS IN SEAWATER

FINAL REPORT

SwRI® Project No. 18.12210
MMS Order No. 0106PO39569

Prepared for:

Minerals Management Service
361 Elden Street
Herndon, VA 20170

Prepared by:

Robert A. Hart
Steven J. Svedeman
Flavia Viana

Approved:

_____
J. Christopher Buckingham
Manager, Multiphase Flow

ACKNOWLEDGEMENTS

ADVERTISING, CONFIDENTIALITY, AND
RECORD RETENTION POLICY

All work related to this project is subject to the Southwest Research Institute® Advertising, Confidentiality, and Record Retention Policy. This policy specifically addresses the distribution of abridged versions of SwRI® reports (including excerpts) and also restricts the use of the SwRI name, logo, and test results for advertising purposes. SwRI policies specifically prohibit the use in advertising of its name, logo, and results provided by our studies. The following paragraph, extracted verbatim from SwRI contractual documents clarifies this point:

> "SwRI shall not publish or make known to others the subject matter or results of the Project or any information obtained in connection therewith which is proprietary and confidential to Client without Client's written approval. No advertising or publicity containing any reference to SwRI, or any of their employees, either directly or by implication shall be made use of by Client or on Client's behalf without SwRI's written approval. In the event Client distributes any report issued by SwRI on this Project outside its own organization, such report shall be used in its entirety, unless SwRI approves a summary of abridgment for distribution."

SwRI will retain a record copy of the report for a period of five (5) years. This permits us to answer questions that may be raised after a report has been mailed and provides a basis for additional work, if required. The contents of the report and any information, which comes into our possession during the course of a study, are held confidential to the company conducting the study and are not disclosed to anyone without client's prior permission.

TABLE OF CONTENTS

LIST OF FIGURES

LIST OF TABLES

LIST OF ACRONYMS

BOP   Blowout Preventer

ELG   Effluent Limitations Guidelines

EPA   Environmental Protection Agency

GOM   Gulf of Mexico

IO   Isomerized Olefin

LAO   Linear-α-Olefin

MMS   Minerals Management Service

OBM   oil-based mud

PAO   Poly-α-Olefin

SBM   synthetic-based mud

WBM   water-based mud

EXECUTIVE SUMMARY

This report describes a project that was conducted to characterize the fall velocity distributions that would result from an accidental release of synthetic-based drilling mud (SBM) in offshore waters. The investigation focused on determining how fall velocity distributions for SBMs used in Gulf of Mexico operations are affected by release conditions. It is expected that the present work will contribute to the understanding of how SBM spills disperse in the marine environment and provide a basis for developing methods to manage such spills

The project included an industry operations survey that showed that Internal Olefin (IO) SBMs with densities in the range of 9-15 lb/gal were the most commonly used muds in Gulf of Mexico drilling operations. The types of spills identified in the survey could be classified as coming from two types of sources: a discharge of fluid overboard and subsea releases. Based on the information gained from the operations survey, it was concluded that for the purposes of this investigation, two general cases, an overboard spill and a release from a submerged jet, could be considered to be representative of the majority of Gulf of Mexico SBM spills.

A literature review and a limited modeling effort was performed to identify existing fluid breakup models from published literature and predict SBM drop size for different SBM release conditions. Understanding fluid breakup mechanisms provides considerable insight into how release conditions affect the resulting fall velocity distributions and how SBM behaves once it enters the seawater.

Two series of fall velocity tests were performed in the SwRI Fall Velocity Test Rig (FVTR). These experiments were intended to represent the two general spill cases identified from the operations survey. A total of five different SBMs were tested in each series of experiments. In the first series, intended to represent an overboard spill, SBM was poured from a container into seawater in the FVTR test section. The case of an underwater release from a pressurized source was simulated by discharging SBM from a submerged jet at various velocities into the FVTR test section. Similar fall velocity distributions for all of the muds were obtained from the overboard spill tests, but the magnitude of the fall velocity depended on the SBM specific gravity. The fall velocity distributions obtained from the submerged jet experiments depended strongly on the jet velocity. As the jet velocity was increased, the fall velocities moved lower due to the formation of smaller droplets. The shape of the fall velocity distributions also changed indicating that the drop size distributions were being altered at the higher jet velocities. Similar trends in the relationship between fall velocity and jet velocity were seen in all of the SBMs tested.

1. INTRODUCTION

As the oil and gas industry continues to seek out new reserves in offshore waters, especially in the Gulf of Mexico, there is a need to better understand how accidental spills of the fluids used in well drilling operations disperse in the ocean. Such an understanding will be important in assessing the impact of spills on the marine environment surrounding the drilling and production platforms and in developing mitigation strategies.

Among the different types of drilling fluids available, synthetic-based muds (SBMs) are commonly used in offshore drilling, especially in difficult wells such as those in deep water or wells with highly deviated wellbores. SBMs combine the desirable operating qualities of oil-based muds (OBMs) with the lower toxicity and environmental impact of water-based muds (WBMs). While SBMs appear to be less toxic to aquatic life and more biodegradable in marine sediments than OBMs[1], it is important to evaluate the dispersibility of SBMs in seawater in order to understand how best to manage accidental discharges.

Because SBMs are immiscible in water, they will tend to form droplets when released into water. SBMs are almost always more dense than seawater, so the resulting droplets will settle toward the seafloor. As they fall in the ocean, smaller, more slowly falling droplets will tend to be dispersed over a wide area as compared to the larger, faster falling droplets that will tend to collect in a region near the release location. Consequently, data on the fall velocity, or terminal velocity, of SBM droplets are a key input to computer models used to predict the fate of spills in the ocean. A given release will tend to produce a range of droplet sizes, and this range will depend on the details of how the material is released as well as the properties of the SBM and seawater. Thus, for a given release, there will be a distribution of fall velocities corresponding to the different sizes of droplets formed. Fall velocity distributions are not well predicted by conventional settling theory (Stokes law) or by knowledge of the droplet size. As a result, experimental determination of fall velocities is needed.

The project described in this report was carried out by Southwest Research Institute (SwRI) at the request of the Minerals Management Service (MMS) of the U.S. Department of the Interior. The purpose of the project was to characterize the fall velocity distributions that would result from an accidental release of various SBMs in offshore waters. The investigation focused on determining how the fall velocity distributions for SBMs used in Gulf of Mexico operations are affected by release conditions. It is expected that the present work will contribute to the understanding of how SBM spills disperse in the marine environment and provide a basis for developing methods to manage such spills.

This project was divided into three major parts: Operations Survey, Droplet Size Modeling, and Experimental Measurements. The remainder of this section discusses the technical background for this project and summarizes some previous research work that is relevant to this topic. Section 2 of this report presents the results of an industry operations survey that was performed to gain a better understanding of the circumstances surrounding recent SBM spills in the Gulf of Mexico. Section 3 contains the results of a literature review and a limited modeling effort that was done to determine what factors affect SBM droplet size. In Section 4, the results of experimental measurements are presented and discussed. Finally, the conclusions resulting from the work performed in this project are summarized in Section 5.

1.1 Mud Circulation System

During the rotary drilling process, drilling fluid (often called drilling mud) is continuously circulated through the well.[2] The drilling mud is pumped from storage tanks (often called pits) by reciprocating pumps that discharge into a series of high-pressure surface connections leading to the drillstring. The mud flows down through the drillstring to the bit where it exits through nozzles built into the bit. The mud then returns to the surface by flowing up the annular space between the drillstring and the well bore. Once at the surface, the mud passes through contaminant removal equipment that includes mechanical devices for separating solids and gases from the mud. The rock debris or cuttings are removed by shale shaker screens before the mud flows back to the storage tank. In addition to the active or suction mud pits, most drilling operations also include reserve mud pits that are used for storage of fresh or excess volumes of drilling mud and for holding contaminated or discarded drilling mud.

In offshore drilling, the drilling fluid is piped between the drilling rig on the surface and the ocean floor through a marine riser, consisting of individual sections between 70-90 feet long. The riser connects to the blowout preventer (BOP) stack through a flex joint that allows lateral movement of the riser. The BOP stack for a floating drilling operation is placed on the ocean floor below the marine riser. It is used to ensure pressure control of the well. The BOP can be closed in case of an emergency, such as a loss of well-control or severe weather conditions.

Lines pressurized with drilling fluid, called kill and choke lines, are connected to the BOP stack and run along the outside of the drilling riser to the surface. These high-pressure flowlines make it possible to flow through the annulus with the BOP closed. The kill line permits drilling fluid to be pumped down the annulus from the surface and the choke line is used to release fluid under pressure from the annulus.

1.2 Drilling Fluids

Drilling fluids serve many different functions during the well drilling process. Some of the main functions of drilling fluids include the following:[3]

- transport of cuttings to the surface

- cooling, cleaning, and lubrication of the drill bit

- maintaining a pressure balance between the geological formation and the borehole

- reduction of friction in the borehole

- sealing of permeable formations

- maintaining stability of the borehole walls

Drilling fluids consist of a combination of a base fluid, water, clay, weighting materials (often barite), emulsifiers, dispersants, viscosifiers, and other rheology modifiers. Other additives may also be included in the drilling fluid, as needed, to adjust the mud properties to meet the needs of a particular drilling operation.

Depending on the type of base fluid used, drilling fluids can be generally classified into three categories: water-based muds (WBMs), oil-based muds (OBMs), and synthetic-based muds (SBMs). WBMs are commonly used for offshore drilling and are generally considered not to be harmful to the marine environment. OBMs offer a number of performance benefits over WBMs that include superior hole stability, thinner filter cake, excellent lubricity, and less risk of stuck pipe.[4] The major disadvantage of OBMs is that the base fluid poses an environmental hazard if it is released into the ocean either through a spill or on cuttings.

More recently, the drilling industry has developed several types of synthetic-based muds that combine the desirable operating qualities of OBMs with the lower toxicity and environmental impact qualities of WBMs.[5] SBMs have drilling and operational properties similar to those of OBM systems and are used where OBMs are commonly used, such as in difficult drilling situations where the properties of WBMs would limit performance (feet drilled per hour). SBMs are well suited to the high-angle, directional, horizontal, and extended-reach wells that are common in multiwell platform sites in the North Sea, the Gulf of Mexico, and elsewhere.[5]

The discharge of waste material from offshore drilling operations is regulated by the U.S. Environmental Protection Agency (EPA), which issues effluent limitations guidelines (ELG). The ELGs prohibit releases of free oil from drilling fluids and drill cuttings discharges.[4] OBMs and OBM cuttings cannot pass the static sheen test used for detection of free oil and thus must be transported to shore for disposal. On the other hand, an advantage of water-based muds is that the drilling fluid itself and the cuttings can usually be discharged into the ocean.[1] Regulations also permit the cuttings obtained from wells drilled using SBMs to be discharged into the ocean if they meet ELGs, but the direct discharge of SBM into the ocean is not allowed, except for the amount retained on the cuttings. Although the purchase costs of SBMs are generally several times higher than the costs of OBMs, the higher costs are offset if cuttings from wells drilled with SBMs can be discharged on site, saving transportation and disposal costs.

1.3 Synthetic-Based Muds

The EPA defines an SBM as a drilling mud in which a synthetic base fluid chemical is the continuous phase with water (brine) as the dispersed phase.[1] Consequently, droplets of SBM will have an outer layer that is immiscible in water. There are several SBM types currently used in the drilling industry. These SBMs are classified according to the molecular structure of the synthetic base fluid.

The base fluids in SBMs are synthesized organic compounds that are essentially immiscible with water. In contrast to OBMs composed of diesel or mineral oils that are refined from crude oil, synthetic fluids are all made from compounds that contain none of the toxic components found in refined oils, such as aromatics and cyclic structures. The most common of these synthetic fluids include the following: Esters, Ethers (the most current version, a di-ether, is more biodegradable than its mono-ether predecessor.), Poly-α-Olefin (PAO), Detergent Alkylate, Linear-α-Olefin (LAO), Isomerized Olefin (IO), and Dimethyl siloxane-based oligomeric siloxanes.[6,7]

These various types of SBMs have a wide range of chemical properties and drilling performance parameters. The environmental impacts from the different SBMs differ as well.[5] Like conventional OBM systems, the formulation of an SBM uses emulsifiers, wetting agents, viscosifiers, and fluid-loss-control agents. Calcium chloride brine (25% to 30% by wt.) is often used to produce the osmotic pressure necessary to stabilize shale, and barite is added to increase mud density. The choice of a particular base fluid is based on many factors such as toxicity, biodegradability, thermal stability, viscosity, cost, and the desired drilling performance and type of application in the field.[7]

The dispersibility in seawater of synthetic fluids has been investigated by Growcock et al.[8] and by Friedheim and Patel.[4] The testing of Growcock et al. was done in shaker flasks by mixing equal amounts of the synthetic fluid and seawater, shaking for 10 seconds, and allowing the mixture to rest for 10 minutes. The amount of synthetic fluid in the water was measured by draining off a certain amount of the water phase and analyzing it with a Total Carbon Analyzer. They reported the following trend in order of decreasing dispersibility:

Esters > Di-Esther >> Detergent Alkylate > PAO > Low-Toxicity Mineral Oil (LTMO).

Friedheim and Patel observed a glycol-ether and an IO SBM after allowing them to set in seawater for three days. They found that the glycol-ether mud dispersed in water, while the IO mud remained intact at the bottom of the container.

2. OPERATIONS SURVEY

An industry survey was performed in order to gain a better understanding of the operational conditions and characteristics of incidents involving the discharge of SBMs. The objectives of this task were to identify the SBM formulations typically used in offshore drilling operations and to collect detailed data on spills such as location and cause. To be consistent with the goals of this project, this survey focused exclusively on operations in the Gulf of Mexico. The data obtained from the survey were used to identify the most common spill scenarios as a basis for defining a general approach for the experimental work that followed.

The survey was done by conducting telephone interviews with people from industry with experience in offshore drilling operations and drilling fluids. The respondents represented both SBM suppliers and personnel involved with drilling. Potential respondents were identified from the MMS database of significant GOM spills[9] and from SwRI industry contacts. Interviews were conducted with representatives from seven different companies. The participating companies were as follows:

- Transocean Inc.

- Shell Offshore Inc.

- Saudi Aramco

- ExxonMobil

- MI Swaco

- Halliburton

- Baker Hughes

Additional information on SBM spills was obtained from the online MMS database on significant ($\geq$ 50 bbl) GOM spills.

2.1 Synthetic-Based Muds Used in the Gulf of Mexico

The results of the survey showed that IO SBMs with densities in the range of 9-15 lb/gal were the most commonly-used muds in the GOM. The fraction of synthetic base fluid contained in SBMs ranged from 50% to 88%. There is not a typical composition of SBM, as the specific formulation of the mud is customized for each project based on the characteristics of the formation to be drilled, temperature range, fracture gradient, pour pressure, casing design, equipment to be used, etc.

A list of the SBMs commonly used during drilling operations in the Gulf of Mexico is given in Table 2-1. In many cases, the driller of a well will contract with a drilling fluid company to supply and handle the SBM and monitor its characteristics throughout the drilling process. At the end of the project, the drilling fluid company will remove the mud, clean it, and recycle it for future projects.

Table 2-1. SBMs Commonly Used in the GOM.

Trade names, description, and suppliers of SBMs that the operations survey showed to be commonly used in GOM drilling.

SBM TRADE NAME	DESCRIPTION	SUPPLIER
Novaplus	Low-viscosity, internal olefin base	MI Swaco
Accolade	Combination of vegetable esters and internal olefin-based fluids	Halliburton - Baroid
Rheliant	Flat rheology, internal olefin-based	MI Swaco
Eco-Mul Synthetic	Olefin-based synthetic mud	Ambar LoneStar

2.2 Locations and Causes of Spills

Spills of SBM can occur from essentially any part of the mud circulation system. Based on information gained in the operations survey, the most common locations and causes of spills are shown in Figure 2-1. In most cases, it was possible to obtain information about the location, estimated fluid volume lost, and cause of a spill, but the exact conditions of the release in terms of flowrate, orifice size, and temperature were usually not known. Survey respondents were also asked about sizes, dimensions, and volumes of some of the major components of the mud circulation system used in offshore drilling. Typical values are summarized in Table 2-2.

LOCATION	CAUSE
Pits, tanks, shale shaker	– Flooding – Valves inadvertently left open
Pipes, hoses, valves, joints	– Leak – Clogged hoses – Valves inadvertently left open
Riser	– Leak at joints – Emergency disconnection
Choke, kill & boost lines	– Leak – Rupture
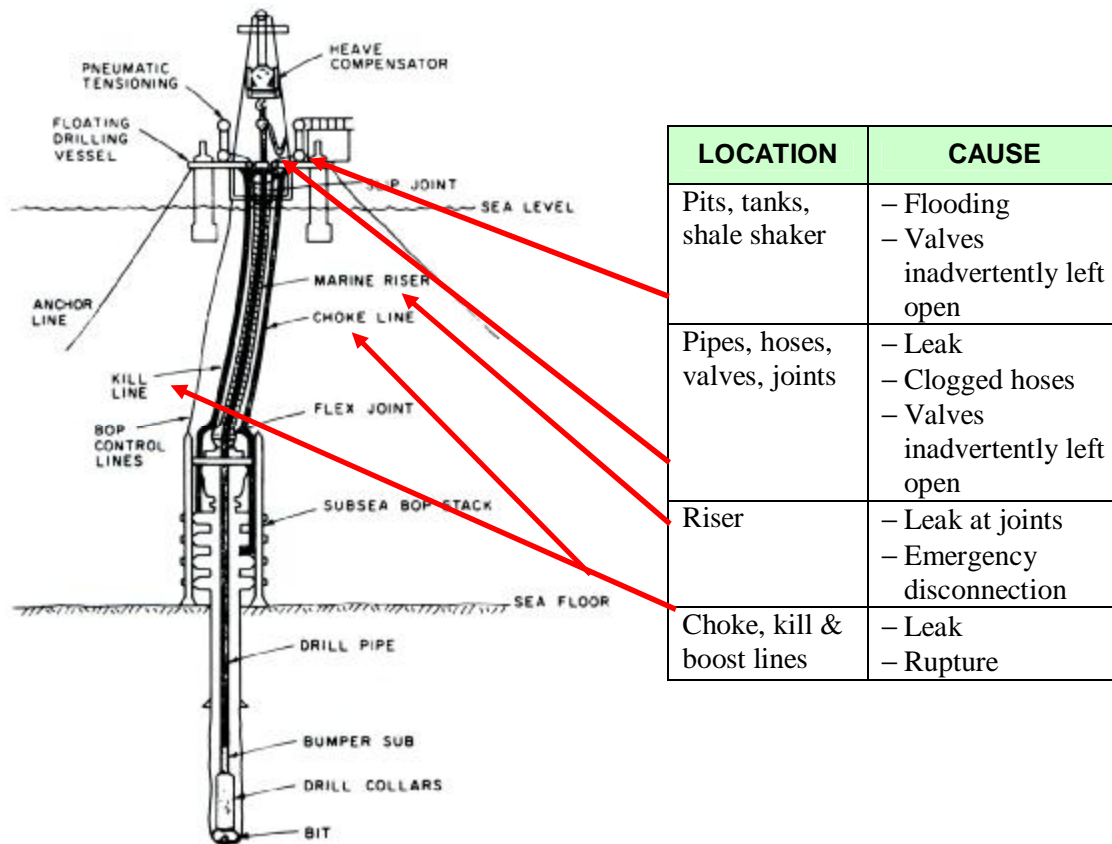
Figure 2-1. Typical Drilling Fluid Release Locations and Causes.

Drilling fluid releases can occur either above the sea surface or from subsea sources as shown on this schematic of an offshore drilling rig (from Bourgoyne et al.[2]).

Table 2-2. Size Ranges of Components Found in the Mud Circulation System.

Information obtained during the operations survey on typical values or ranges of values for offshore drilling mud circulation system components.

PARAMETER	TYPICAL VALUE OR RANGE
Riser outer diameter	20 in. – 24 in.
Riser wall thickness	13/16 in. for a 21-in. OD riser
Temperature of the fluid	40°F (if fluid remains long enough inside a submerged line) to 350°F
Drill-pipe OD	3 in. - 5 in.
Kill and choke lines ID	3 in. - 6 in.
Kill and choke lines maximum pressure	15,000 psi
Boost line ID	4 in. - 6 in.
Boost line maximum pressure	5,000 psi - 6,000 psi
Flowrate in the mud circulation system	300 gpm – 1,400 gpm
Active mud system	Consists of 6 to 12 pits of about 500 bbl each
Reserve mud system	Consists of 5 or 6 1,500-bbl pits

The MMS investigates significant spill incidents of 50 bbl (2,100 gal) or more that occur during offshore drilling operations and publishes this information on its website. Data on GOM-reported spills for 2002-2006 were analyzed to determine causes and locations. During this period, there were 27 reported spills with an estimated total of 9,302 bbl of base fluid lost. Note that this is only the amount of synthetic base fluid spilled, not the total volume of drilling mud spilled, which will be larger. The volume of base fluid was calculated from the reported SBF fraction for each spilled mud.

For comparison purposes, the MMS SBM spill data were broadly classified into three categories based on the locations from which the releases occurred. These categories and typical causes in each category are as follows:

- **Overboard** – These were spills in which drilling fluid was released above the water surface and fell into the ocean. The most common reported causes of overboard spills include valves left open, valves that fail to seal when closed, clogged lines, overflow of mud pits or shale shaker, and inadvertent discharges. Many of these spills were attributed to human errors.

- **Subsea** – These are releases of drilling mud that occur somewhere under the surface of the water. The most common reported causes of subsurface spills are leaks or ruptures of pressurized lines, such as the kill line or leaks at riser joints.

- **Seafloor** – This category encompasses spills that occur very near the seafloor. Most commonly this is caused by the emergency disconnection of the drilling riser due to adverse weather conditions or leaks at the BOP or wellhead.

Figure 2-2 shows the results of the analysis of the reported spill data. Releases at the seafloor account for the largest volume of SBM spilled, with about equal amounts attributable to the other two categories (subsea and overboard). The large volume for seafloor releases is due to the fact that this category includes several emergency riser disconnects that tend to spill a large amount of fluid per incident. Viewing the data in terms of the number of occurrences of each type reveals that overboard spills occur much more frequently than other types.
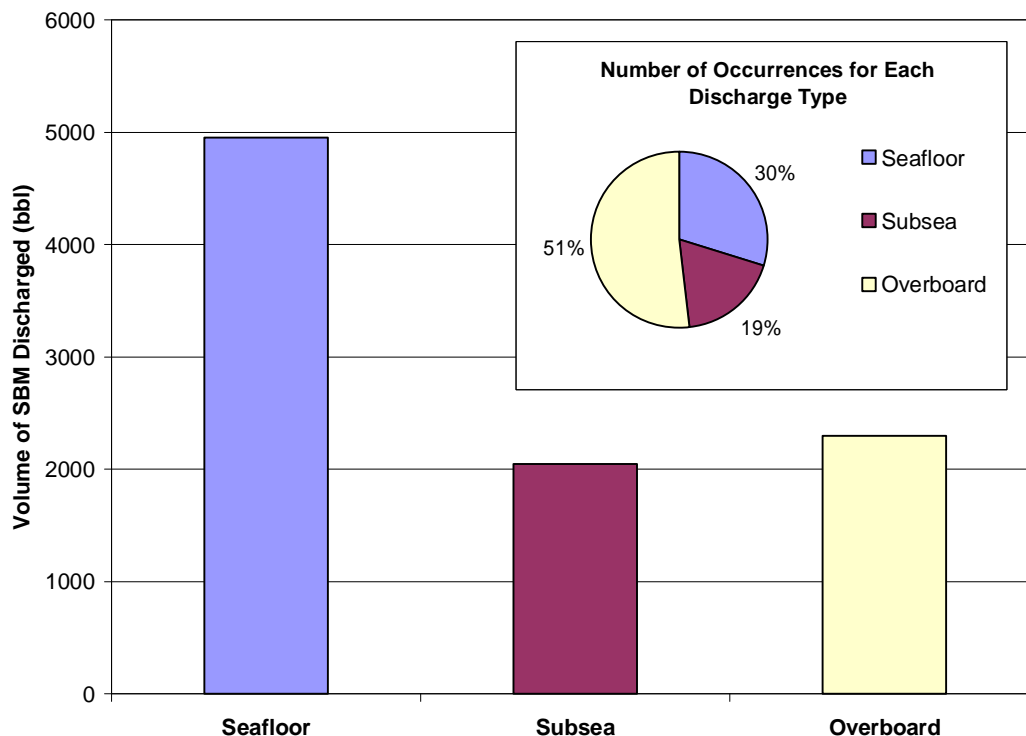
Figure 2-2. Number of SBM Spills and Volumes Discharged for Releases in the Gulf of Mexico Larger than 50 bbl for the Years 2002-2006.
Excluding releases near the seafloor, subsea and overboard sources account for about the same amount of fluid lost, but overboard spills occur much more frequently.

2.3 General Approach

The variety of SBM formulations available, coupled with the many possible sources of spills, creates an intractably large range of test conditions to cover in an experimental investigation. Furthermore, the source of a spill, such as the rupture of an undersea line or a leak at a connection, can be very difficult to characterize and replicate in the laboratory. For these reasons, and to keep the project scope reasonable, it was necessary to limit the investigation to a number of idealized cases. The choice of representative test cases was guided by the results of the operations survey and the modeling work, which will be described later.

The information obtained in the operations survey suggests that SBM spills can be considered to come from two generic sources: a discharge of fluid overboard and subsea releases. When a spill occurs above the water surface, as would happen when drilling fluid is lost overboard, the SBM will fall through the air and enter the water where it will break up into droplets as it settles toward the ocean floor. On the other hand, when a leak or rupture occurs in a subsea pressurized line, a jet of SBM is introduced into the surrounding seawater and this

liquid jet disintegrates into individual droplets. In either case, as the SBM moves away from the spill source, the droplets would be expected to undergo some size changes before reaching a stable, steady state size. The range of droplet sizes formed will determine the fall velocity distribution for a particular situation.

The general approach taken in this project was to consider the above two general cases (overboard spill and submerged jet) to be representative of the majority of GOM SBM spills. The situation where SBM is released near the seafloor was sufficiently different from the other spill cases that it was considered to be outside the scope of this project. For spills close to the seafloor, the SBM will likely accumulate in a localized region on the seafloor and will not be subjected to the type of dispersal that would occur if the fluid were settling in the ocean due to a release farther up from the seafloor. In these cases, dispersal is likely to be governed more by ocean dynamics than by the details of release.

3.   SBM DROP SIZE MODELING

The objective of this task was to identify existing fluid breakup models from published literature and use the models to predict SBM drop size for different SBM release conditions. Although the focus of this project is on fall velocity, and not drop size, understanding fluid breakup mechanisms provides considerable insight into how release conditions affect the resulting fall velocity distributions and how SBM behaves once it enters the seawater. This limited modeling effort was used to guide the design of the experimental work by providing information about the important range of parameters (nozzle diameter, jet velocity, SBM properties) and expected drop sizes.

As discussed in the preceding section, two different spill scenarios are envisioned, an overboard spill and a release from a submerged jet. In either case, the SBM will break up into droplets as it falls through the water. An upper bound on the drop size (maximum stable drop size) is set by the drop size that is stable at the drop terminal (fall) velocity. If the drops formed during the spill event are larger than the maximum stable drop size, they will break up into successively smaller drops until they reach a size consistent with their fall velocity. In the case where the SBM is discharged from a submerged jet with sufficient velocity, the drop size will be governed by the breakup of the fluid in the high velocity jet. Drops formed in this manner may be initially smaller than the maximum stable drop size.

3.1   Maximum Stable Drop Size

The maximum stable size for a drop is determined by the interfacial tension force holding the drop together versus the drop deformation caused by buoyant flow. The method of Grace, Wairegi, and Brophy[10] can be used to determine the maximum stable drop size for immiscible drops in a stagnant fluid. The breakup of a drop in stagnant fluid is predicted with a two-dimensional Rayleigh-Taylor stability theory. The drop will break up if indentations on the drop's leading edge grow fast enough compared to the speed that the disturbance is carried around the bubble. Calculating the maximum stable drop size requires iterative calculations, since the maximum drop size depends upon the drop velocity and the drop velocity depends upon the drop size.

The correlations of Clift et al.[11] can be used to estimate the fall velocity of non-spherically shaped drops. Figure 3-1 shows the computed terminal velocity of oil drops (specific gravity 0.8 and viscosity of 2 cP) in seawater using Clift's correlation. The terminal velocity of a solid spherical particle is also shown on the plot for comparison. At the smaller diameters, the drop surface tension maintains a spherical shape and the drop fall velocity is equal to the velocity of an equivalent density solid spherical particle. At drop equivalent diameters (diameter of the volume equivalent sphere) over about 0.5 cm, the terminal velocity of the drop is reduced because the oil drop deforms and drag is increased compared to a spherical particle. Clift's drop velocity correlation can be used with Grace's method for predicting maximum stable drop size in buoyant flow.
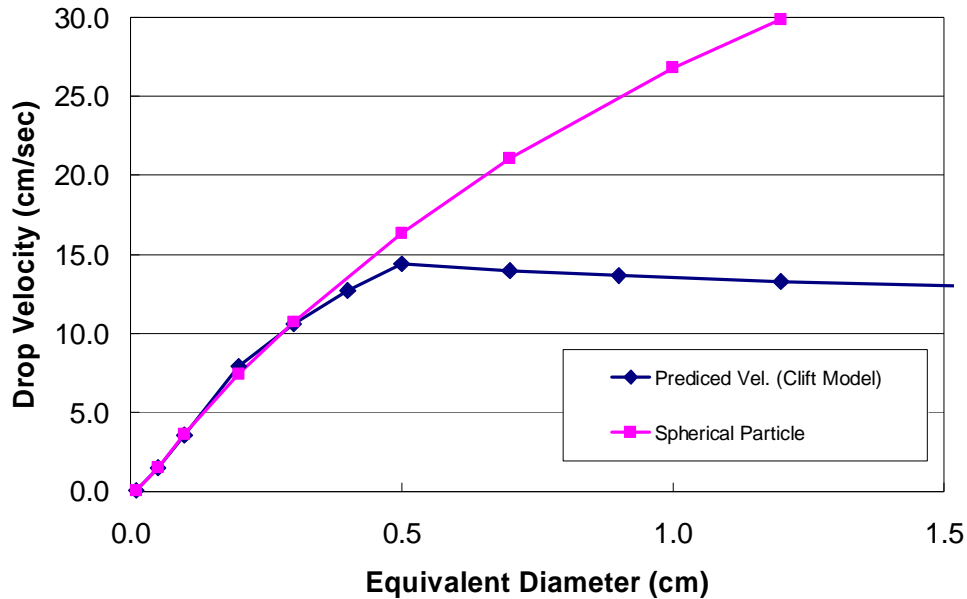
Figure 3-1. Terminal Velocity of Oil Drops and Equivalent Density Solid Spheres in Water.
The terminal velocities of drops larger than about 0.5 cm are limited by droplet deformation.

The drop breakup model of Clift was used to establish the largest drop sizes expected for a range of conditions. Figure 3-2 and Figure 3-3 show examples of the maximum stable drop diameter (in seawater) as a function of the drop viscosity and drop specific gravity (specific gravities of 1.2, 1.5, and 1.8 correspond to drop densities of 10.0 lb/gal, 12.5 lb/gal, and 15.0 lb/gal respectively). Figure 3-2 is for an interfacial tension of 30 dyne/cm and Figure 3-3 is for an interfacial tension of 10 dyne/cm. The strange looking shapes of the curves (they are not smooth curves) correspond to transitions between different droplet shapes. The graphs show that drops with a volume equivalent diameter of up to 4 cm can be stable if the drop viscosity is very low. For drop viscosities more typical of drilling fluid (> 10 cP), the maximum stable drop diameter is limited to less than 2 cm.

As would be expected, the graphs in Figure 3-2 and Figure 3-3 show that lower drop specific gravities produce larger maximum stable drop sizes. This is because the smaller density difference between the drop and the seawater produces a lower drop fall velocity. This lower drop fall velocity allows larger drops to remain stable. Also, comparing both Figure 3-2 and Figure 3-3 shows the effect of interfacial tension on the maximum stable drop size. The maximum stable drop size for a 1.2 specific gravity drop changed from 4 cm to 2.4 cm for an interfacial tension change from 30 dyne/cm to 10 dyne/cm.

The fall velocities that correspond to the drop sizes shown in Figure 3-2 and Figure 3-3 are shown in Figure 3-4 and Figure 3-5. For drop viscosities over 10 cP, the maximum drop fall velocity is less than 20 cm/sec.

It should be noted that these calculations were based on models for Newtonian fluids, not non-Newtonian fluids like the SBMs. These results, therefore, only provide estimates of the maximum drop sizes and drop fall velocities for a non-Newtonian fluid falling through a water column. No information was found in the literature that predicts the drop size distribution that results from non-Newtonian drops breaking up as they fall through a fluid column.
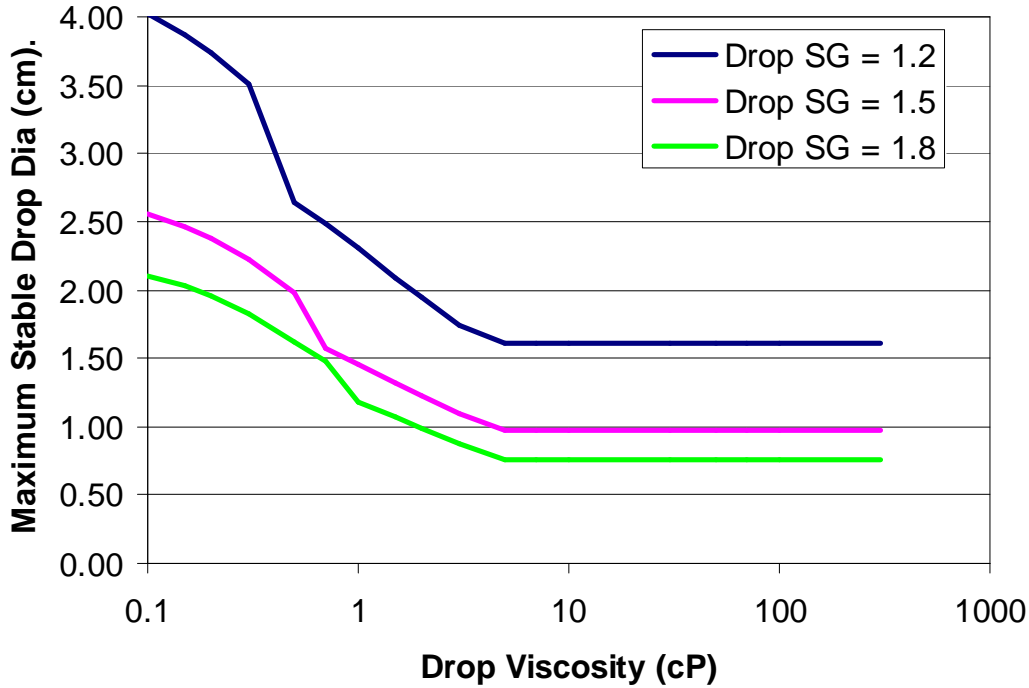
Figure 3-2. Maximum Stable Drop Size as a Function of Drop Viscosity for Different Drop Specific Gravities and an Interfacial Tension of 30 dyne/cm.

Drops as large as 4 cm in diameter can be stable if the density difference between the drop and the seawater is relatively small. For the higher values of the drop viscosity, the maximum stable drop diameter is independent of viscosity.
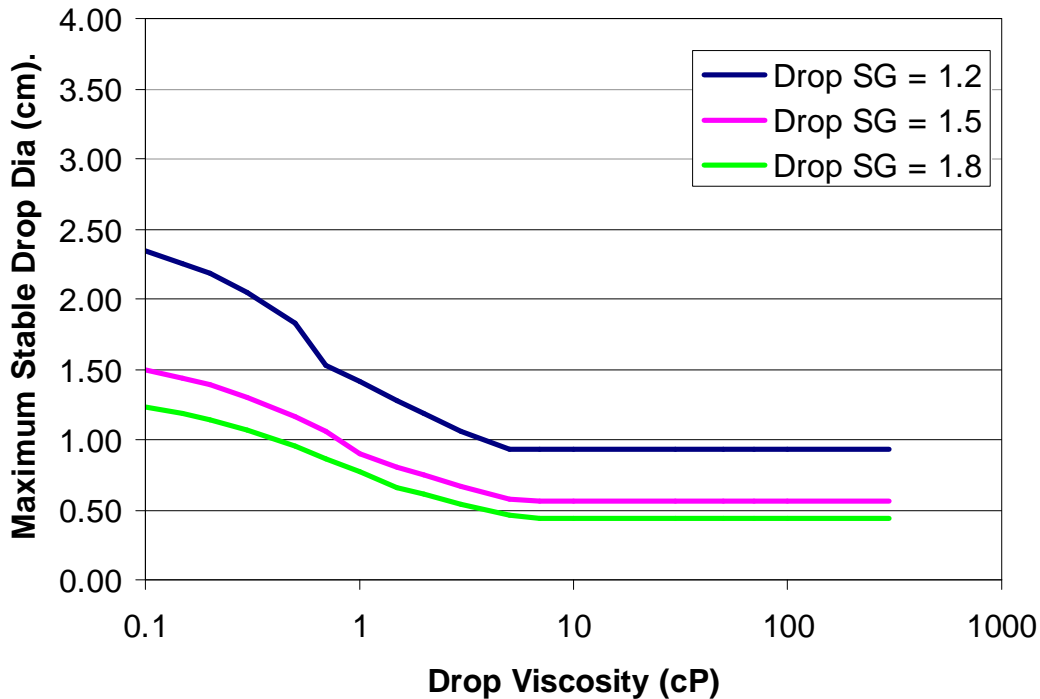
Figure 3-3. Maximum Stable Drop Size as a Function of Drop Viscosity for Different Drop Specific Gravities and an Interfacial Tension of 10 dyne/cm.

The effect of changing the interfacial tension from 30 dyne/cm to 10 dyne/cm can be seen by comparing the results of Figure 3-2 with this figure. The maximum stable drop diameter is reduced from about 4 cm to 2.4 cm.
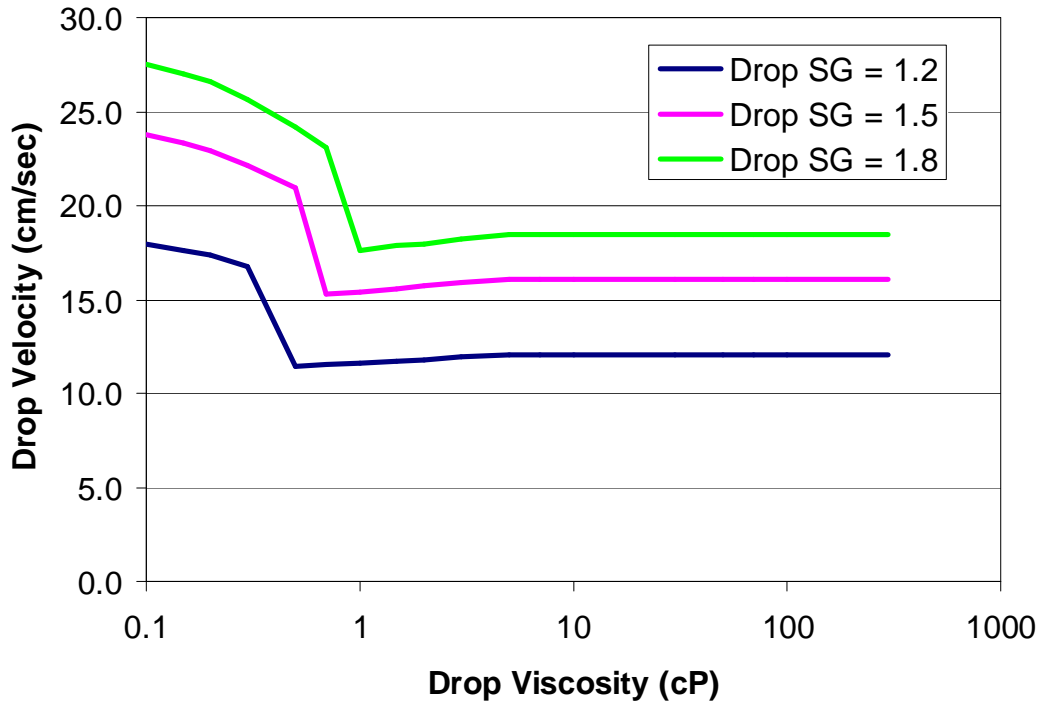
Figure 3-4. Terminal Drop Velocity for the Maximum Stable Drop Sizes Shown in Figure 3-2.
The terminal velocity of drops larger than about 0.5 cm is limited by droplet deformation.
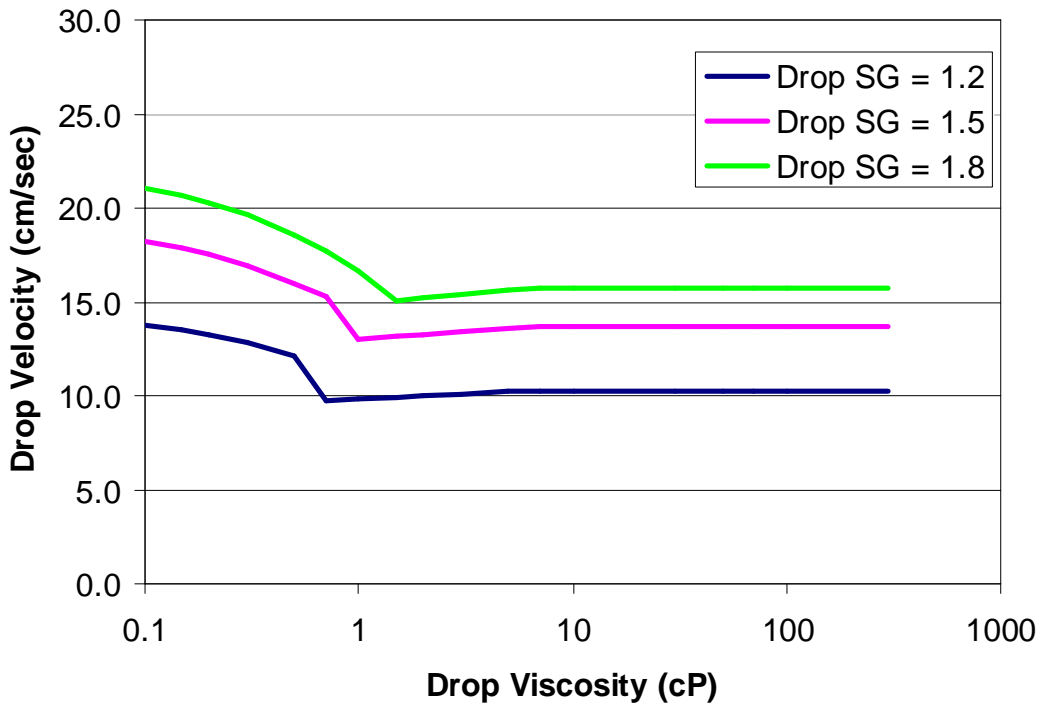
Figure 3-5. Terminal Drop Velocity for the Maximum Stable Drop Sizes Shown in Figure 3-3.
The terminal velocity of drops larger than about 0.5 cm is limited by droplet deformation.

3.2   Submerged Jets

The drop sizes formed from a submerged jet of immiscible liquid depends upon the jet velocity, jet diameter, and the fluid properties. Different jet breakup regimes have been identified with different breakup mechanisms dominating in the different regimes. At very low jet velocities, large drops form at the jet exit or drops are created from a laminar jet of fluid in which Rayleigh instabilities grow to pinch off the jet into individual drops. This jet breakup regime is called Rayleigh breakup, or laminar breakup, and the drops formed have a fairly uniform size. At higher jet velocities, the jet breaks up into a spray of fine drops that have a wide size distribution. In the spray or atomization regime, the breakup mechanism switches from a surface tension dominated breakup (Rayleigh breakup) to one dominated by fluid momentum and viscous forces.

Figure 3-6 shows an example of the drop size and jet length in the different breakup regimes for a water jet discharging into carbon tetrachloride.[12] In this figure, the bars around the drop size indicate the range of drop diameters resulting from the breakup of the fluid in the jet. The Rayleigh breakup region is to the left of the first vertical dashed line (at jet velocities less than about 25 cm/sec). The atomization breakup regime is to the right of the second dashed vertical line (at jet velocities greater than about 55 cm/sec). There is a transition regime located between the Rayleigh and atomization breakup regimes.
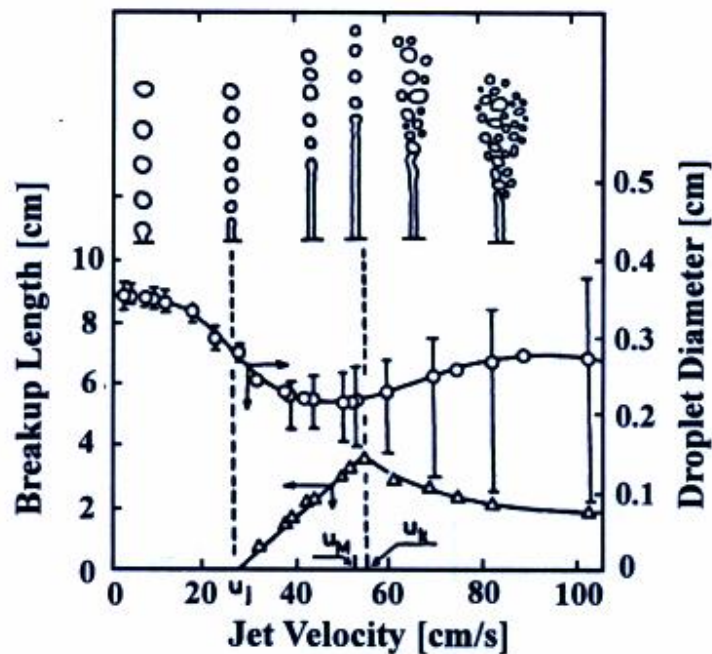
Figure 3-6. Graph Showing the Different Jet Breakup Modes as a Function of Jet Velocity (from Kitamura and Takahashi[12]). The Data are for a Water Jet Flowing into Carbon Tetrachloride from a 0.118 cm Diameter Jet.
At low jet velocities, large uniform drops are formed. At higher jet velocities, the jet breaks up into smaller drops.

The transitions between the different jet breakup regimes depend not only on the jet velocity as seen in Figure 3-6, but also on the fluid properties. Correlations for the breakup

regimes have been developed based on limited sets of experimental data. The correlations are based on the jet Reynolds number (Re_D) and the Ohnesorge number (Z), which are defined as:

$$\text{Re}_D = \frac{r_j V_j D}{m_j} \qquad\qquad Z = \frac{m_j}{\sqrt{r_j s D}}$$

where the subscript j refers to the jet fluid properties, D is the jet diameter, V is the average velocity, ρ is the density, μ is the viscosity, and σ is the interfacial tension.

Figure 3-7 shows the jet breakup regimes experimentally determined for a liquid CO_2 jet in water[13] and for a crude oil jet flowing into water.[14] For the crude oil tests (which have fluid properties closer to SBM than the CO_2 tests, although the oil is Newtonian), the boundaries between the Rayleigh and transition regimes and between the transition and atomization regimes are defined as:

$$Z = \frac{12}{\text{Re}_D^{1.24}} \qquad\qquad Z = \frac{63}{\text{Re}_D^{1.26}}$$

The transitions are based on experimental data from 0.1-cm, 0.2-cm, and 0.5-cm diameter jets, oil densities from 0.88 to 0.98, oil viscosities from 13 cP to 196 cP, interfacial tension of about 25 dyne/cm, and seawater as the ambient fluid. These correlations can be used to determine the type of jet breakup expected for a given fluid system, orifice diameter, and flowrate.
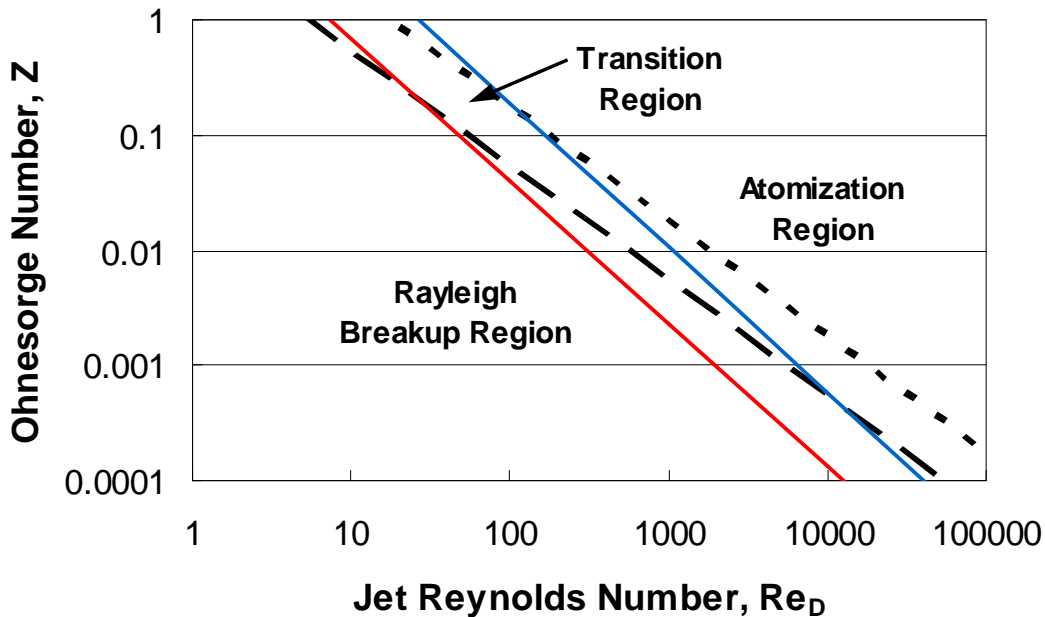
Figure 3-7. Jet Breakup Regimes Shown as a Function of Reynolds Number and Ohnesorge Number.
The correlation shown with dashed lines is for a CO_2 jet in water[13] and the correlation shown with the solid lines is for a crude oil jet in water.[14]

3.2.1 Low-Velocity Jets (Rayleigh Jet Breakup)

The drops formed from the Rayleigh breakup of a low-velocity jet have a fairly uniform drop size. Teng et al.[15] presents a correlation to predict the droplet size for low-velocity jets submerged in a liquid. The drop diameter is given by:

$$d = 1.88 D \left(1.1303 + 0.0236 \ln Z^*\right)\left(1 + Z^*\right)^{1/6}$$

where Z^* is a modified Ohnesorge number. The modified Ohnesorge number includes the ambient fluid viscosity, μ, and is defined as $Z^* = (3\mu_j + \mu)/(D\sigma\rho_j)^{0.5}$. The above equation shows that the predicted drop size for Rayleigh jet breakup is independent of the jet velocity.

An example of the predicted drop sizes for different jet diameters and fluid viscosities is shown in Table 3-1. Fluid density and interfacial tension are not included as variables since the predicted drop diameter is not a strong function of either of these parameters. Note that very low flowrates are required to stay in the Rayleigh jet breakup regime (Re_D must be less than $(12/Z)^{(1/1.24)}$). The last column in Table 3-1 shows the maximum jet flowrate to maintain Rayleigh jet breakup.

Table 3-1. Drop Size Predictions for Different Jet Diameters and Jet Fluid Viscosities.
The calculations were for a jet fluid with a density of 1.5 g/cm³ and an interfacial tension of 30 dyne/cm. The ambient fluid was seawater.

JET DIAMETER (cm)	JET FLUID VISCOSITY (cP)	DROP DIAMETER (cm)	OHNESORGE NUMBER, Z	MAXIMUM REYNOLDS NUMBER, Re_D	MAXIMUM JET FLOW (gpm)
0.1	1.0	0.20	0.0047	558.0	0.0046
0.1	10.0	0.21	0.0471	87.1	0.0072
0.1	100.0	0.25	0.4714	13.6	0.0113
0.1	1,000.0	0.35	4.7140	2.1	0.0176
0.5	1.0	0.96	0.0021	1,067.7	0.0443
0.5	10.0	1.01	0.0211	166.7	0.0692
0.5	100.0	1.14	0.2108	26.0	0.108
0.5	1,000.0	1.54	2.1082	4.1	0.169
1	1.0	1.90	0.0015	1,412.0	0.117
1	10.0	2.00	0.0149	220.5	0.183
1	100.0	2.22	0.1491	34.4	0.286
1	1,000.0	2.91	1.4907	5.4	0.446
2	1.0	3.78	0.0011	1,867.3	0.310
2	10.0	3.97	0.0105	291.6	0.484
2	100.0	4.34	0.1054	45.5	0.756
2	1,000.0	5.52	1.0541	7.1	1.18

The drop sizes predicted for the 1-cm and 2-cm diameter jets are larger than about 2 cm in diameter. As discussed in subsection 3.1, any drops larger than about 2 cm in diameter (for viscosities above 10 cP) that form at a jet will break up under buoyant flow. Therefore, Rayleigh jet breakup may only be of interest for SBM releases where the jet diameter is smaller than 1 cm in diameter. For jets smaller than 1 cm, drops can be formed that will maintain a stable drop size under buoyant flow conditions.

It should be noted that while the Teng equation was based on a fairly wide range of fluid properties, it was only compared to data for orifice diameters that were less than or equal to 0.122 cm. It is not known if this equation provides reasonable results for larger diameter orifices. Teng did include some test data for non-Newtonian jet fluids in the development of his equation, so the drop size equation would be expected to be applicable to some non-Newtonian fluids.

3.2.2 High-Velocity Jets (Atomization Jet Breakup)

In contrast to low-velocity jets, a high-velocity jet will produce droplets with a range of sizes. There are no general correlations that satisfactorily predict the drop size distribution generated by a high-velocity jet.[12] The drop size produced from a laminar jet (Rayleigh jet breakup) can be used as an upper drop size limit for high-velocity jets since drop size decreases with increasing jet velocity.

Rye[16] performed a literature survey on the drop size formed from submerged oil jets. He did not find any suitable correlations to predict drop sizes for the atomization regime.[17] Rye proposed the following provisional breakup model for an oil jet released into the sea:[18]

$$d_{95} = kDWe^{-0.6}$$

where d_{95} is the characteristic drop diameter where 95% of the total liquid volume is in drops of smaller diameter, k is a coefficient (=20), and We is the Weber number ($We=V_j^2 D\rho_j/\sigma$). This correlation does not include any effects for the fluid viscosity or the density difference between the jet and ambient fluids. However, unlike the equation for Rayleigh breakup, it does include the effect of jet velocity through the Weber number. Using the Rye equation, the droplet size distribution is calculated using a Rosin-Rammler distribution with the equation:

$$Q(d) = 1 - \exp\left[-2.996\left(\frac{d}{d_{95}}\right)^p \right]$$

where Q(d) is a fraction of the total fluid volume contained in drops of diameters less than d, and p is the distribution spread constant taken to be 2.5.

Using the above equation, the d_{95} drop size for a submerged SBM jet can be predicted. Figure 3-8 and Figure 3-9 show plots predicting the d_{95} drop size for a range of jet velocities and jet diameters for interfacial tensions of 30 dyne/cm and 10 dyne/cm. As would be expected, the drop size decreases with decreasing jet diameter and increasing jet velocity. For jet velocities of about 250 cm/sec, the maximum drop size is slightly less than 0.5 cm. For jet velocities above 1,000 cm/sec, the maximum predicted drop diameter is less than 0.1 cm.

Figure 3-8 and Figure 3-9 only show the maximum (d_{95}) drop size from a submerged jet, but not the range of expected drop sizes. The drop size range is given by the Rosin-Rammler drop size distribution function and is shown in Figure 3-10 as a normalized drop diameter (d/d_{95}) versus the cumulative volume fraction. For example, for a d_{95} of 0.2 cm, only 1% of the total

drop volume is predicted to be in drops with a diameter less than 0.02 cm, and only 1% of the drop volume would be in drops larger than 0.24 cm.
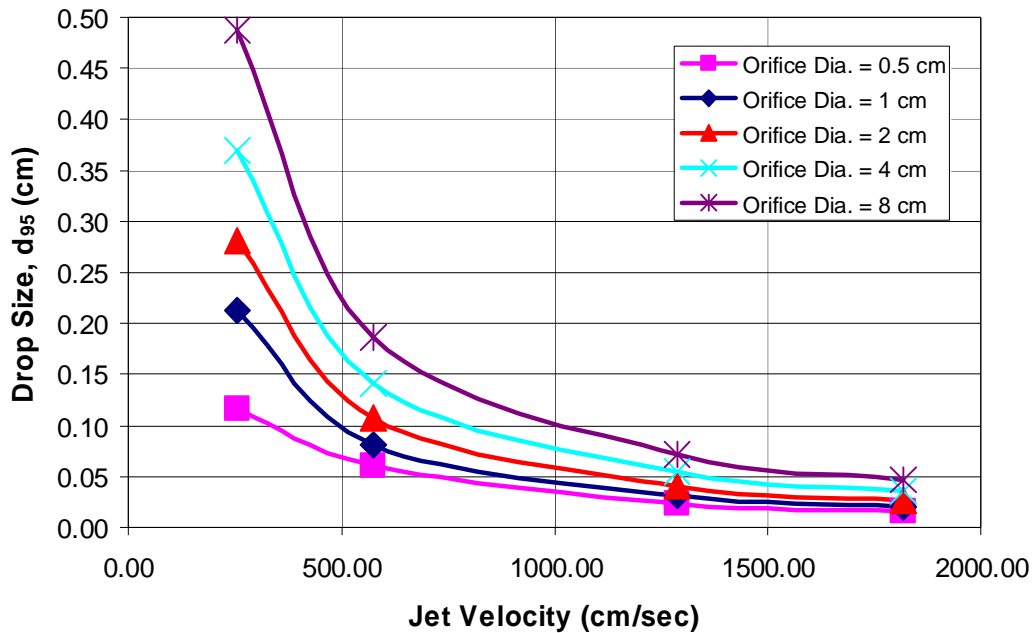
Figure 3-8. Drop Size Predictions for Jets Submerged in Seawater using Rye's Correlation.[18]
The calculations were for a 1.5 g/cm^3 jet fluid with an interfacial tension of 30 dyne/cm.
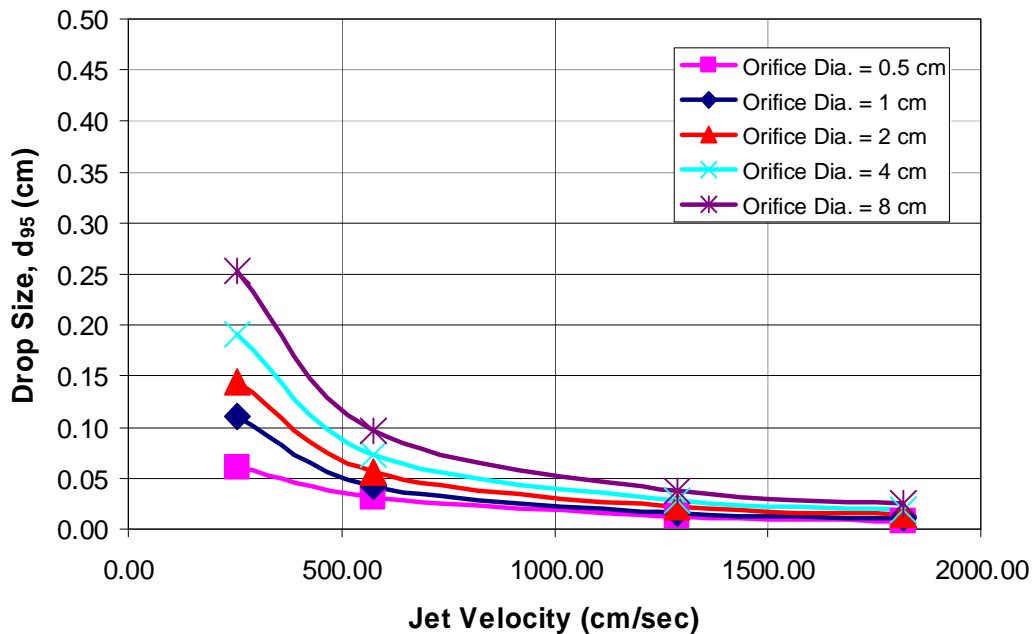
Figure 3-9. Drop Size Predictions for Jets Submerged in Seawater using Rye's Correlation.[18]
The calculations were for a 1.5 g/cm^3 jet fluid with an interfacial tension of 10 dyne/cm.
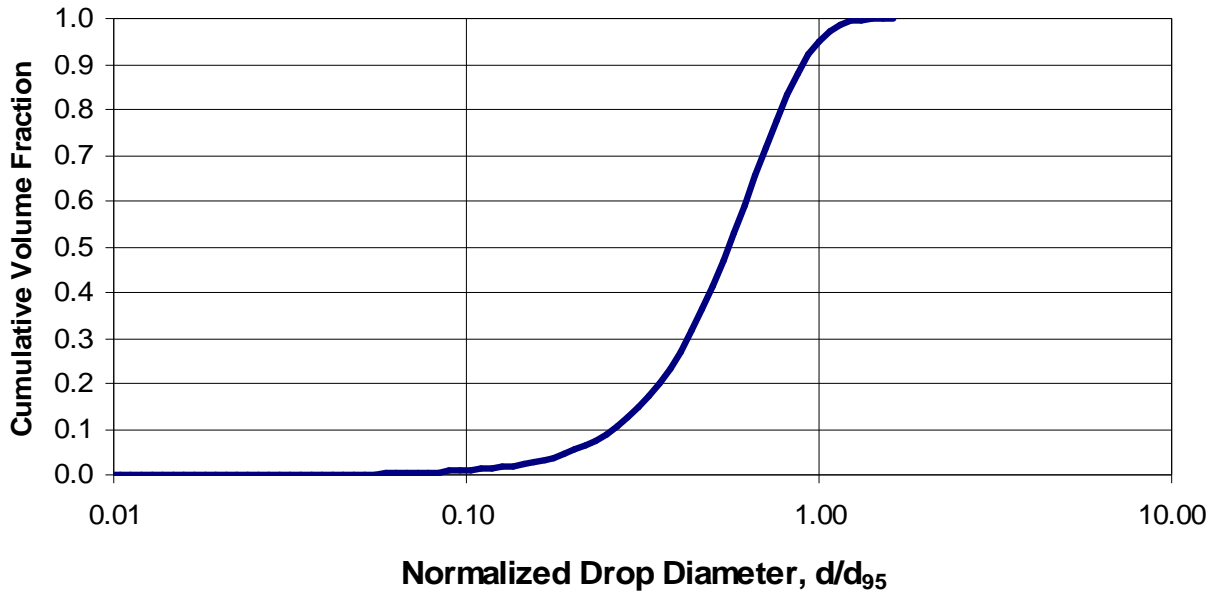
Figure 3-10. Drop Size Distribution Predicted by the Rye Correlation.[16]
The drop diameter is normalized by the d_{95} value, so this plot can be used to determine the range of expected particle diameters for any d_{95} value.

Schroder et al.[19] also developed a correlation for the drop size and drop size distribution resulting from a jet breakup in the spray or atomization regime. The correlation is based on experimental data for oil jetting into water from small diameter orifices (0.3 mm to 0.8 mm). The correlation given for the median drop size, d_{50}, is:

$$d_{50} = 73.2 \cdot D \cdot We^{-0.687} \left(\frac{r_j}{r} \right)^{4.4} \left(Re \frac{m_j}{m} \right)^{0.064}$$

Figure 3-11 shows the predicted drop size using the above equation for the same jet conditions used in Figure 3-8. The correlation of Schroder predicts about an order of magnitude larger drop diameter than the correlation suggested by Rye (comparing d_{50} to d_{95}). This discrepancy may be partly attributable to the fact that the conditions modeled in Figure 3-11 are considerably different from the test conditions that Schroder used to develop the drop size correlations. The correlation was based on orifice diameters less than 0.08 cm and the jet exit velocities were all over 4,800 cm/sec. Schroder's drop size prediction correlation may not provide accurate results for a larger diameter jet with lower jet velocities. No good data sets were found to compare the models for larger jet diameters.

Masutani and Adams[14] reported that the drop size distributions for silicone oil discharging into water in the atomization and transition flow regimes presented bimodal drop size distributions (i.e., there were two separate peaks in the distribution), and thus did not follow the Rosin-Rammler distribution. Tang et al.[13] also reported bimodal drop size distributions in their experiment with liquid CO_2 drop breakup in the transition regime. These results suggest that there may be two different breakup mechanisms occurring in the jet. The small drops are generated from the surface of the jet and the larger drops are generated in the jet core. The data from Schroder et al.[19] did not show the bimodal distribution. However, Schroder's tests were

conducted with smaller jets at much higher velocities than the tests of Masutani and Adams. In addition, Schroder's tests were conducted almost entirely in the atomization regime, while Masutani and Adams ran tests that were in the transition and atomization breakup regimes. This may account for why Schroder did not observe a bimodal drop size distribution.
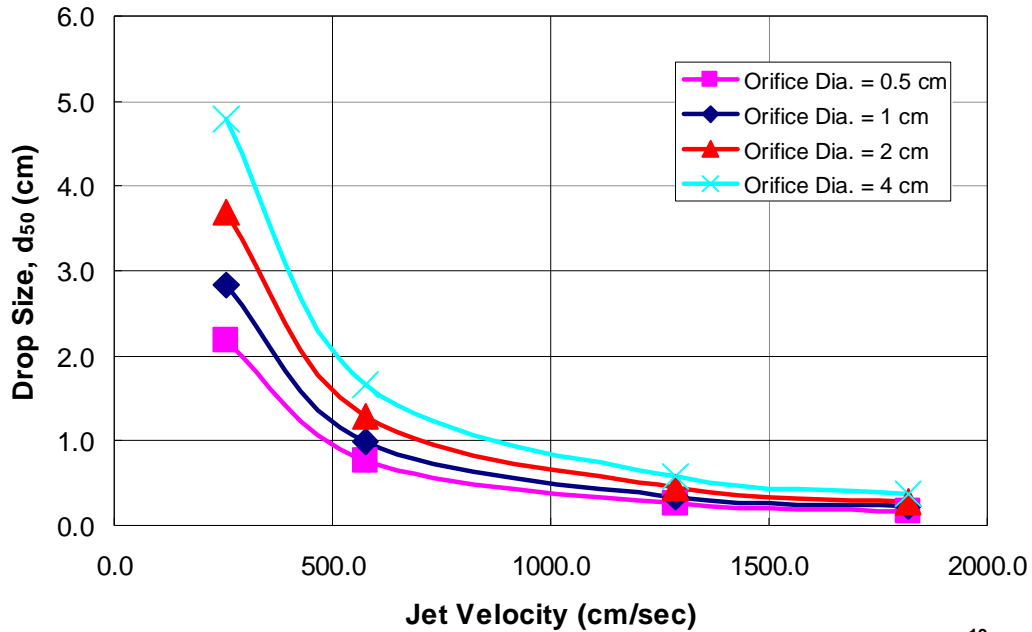
Figure 3-11. Drop Size Distribution Predicted by Schroder's Correlation.[19]
Schroder's correlation predicts much larger drops compared with the Rye correlation.

4. FALL VELOCITY EXPERIMENTS

The basic approach in this project was to conduct fall velocity experiments that were representative of the two SBM spill scenarios (overboard spill and submerged jet) discussed in subsection 2.3. A series of experiments corresponding to each spill scenario was performed to determine the distribution of fall velocities that results when synthetic-based mud (SBM) is released in seawater.

The experimental work was performed using the SwRI Fall Velocity Test Rig (FVTR). The FVTR has been used in a number of previous projects to study the fall velocity of drilling fluids and cuttings. In the first series of tests, intended to represent an overboard spill, SBM was poured from a container into seawater in the FVTR test section. The case of an underwater release from a pressurized source was simulated by discharging SBM from a submerged jet into the FVTR test section. Although a leak in the field could come from an orifice with practically any shape, a round nozzle was used for the jet in the experiments. To allow the droplets to reach a more stable size that will be representative of what will occur as they fall in the ocean, the experiments were performed in a 15-foot high column.

For both spill scenarios, experiments were performed with five different SBMs, and, for the submerged jet case, tests were performed at several jet velocities. Based on the results of the Operations Survey, all of the experiments were performed with Internal Olefin (IO) SBMs with densities in the range 9-15 lb/gal, as these are the most typical specifications for muds used in Gulf of Mexico drilling operations.

The intent of the experimental investigation was to perform some laboratory-scale experiments to gather basic data on SBM fall velocities. Although these experiments will not replicate the conditions found in the field, it is expected that the results from the small-scale (as compared to field conditions) idealized cases will provide insight into what might occur in a real SBM spill.

4.1 Droplet Size and Fall Velocity

For the purposes of determining how SBM would disperse in seawater, it is possible to characterize a spill either in terms of the size of the droplets produced or the fall velocity distribution of the resulting droplets. From discussions with industry contacts familiar with ocean dispersion modeling, it appears that fall velocity distributions and not droplet sizes are the input needed for most models.

If droplet sizes were measured in the experiments, some type of correlation would be needed to predict the fall velocity of the various sized drops. One such correlation for the fall velocity of oil drops in seawater given by Clift et al.[11] was presented in subsection 3.1. As discussed in that subsection, droplets above a certain size do not behave as solid spheres and their fall velocity becomes a function of how the droplet deforms in response to the forces acting on it and the interfacial tension. An example of relatively large SBM droplets from the present experiments is shown in Figure 4-1. These droplets were mostly disc-shaped and many appeared to rock back and forth as they settled in the seawater.
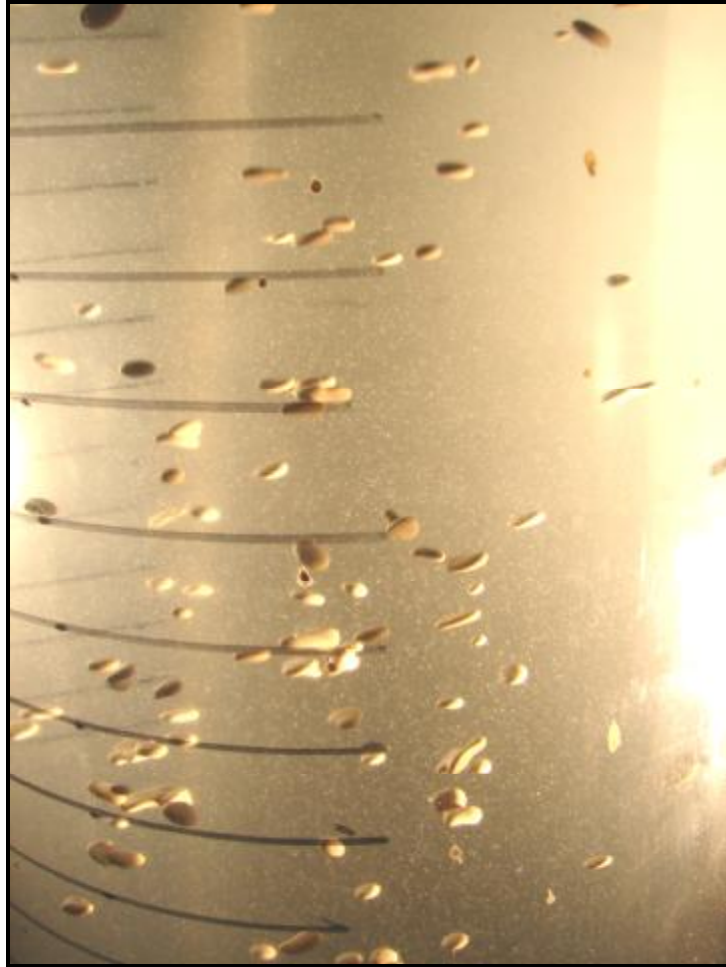
Figure 4-1. SBM Droplets Falling in Seawater.
These relatively large droplets do not maintain a spherical shape as they fall.

Using the relationship given by Clift would likely not yield very good results for SBM droplets as the fluid properties (especially interfacial tension) are different and the correlation was developed for oil, which is a Newtonian fluid (unlike SBM which in non-Newtonian). Consequently, additional experiments would be needed to define the fall velocity/drop size relationship for SBM. To avoid the additional uncertainty created by using such a correlation, the approach adopted in the present project was to measure the SBM fall velocity distributions directly in the experiments rather than droplet sizes.

4.2 Experimental Facility and Methods

All of the experiments for this project were performed in a large settling column that was designed to measure the fall velocity distribution of an SBM sample and allow for observation of the SBM as it fell through the water in the column. This column and its associated equipment, called the Fall Velocity Test Rig (FVTR), are shown in Figure 4-2. The main component of the FVTR is a clear vertical test section that is filled with simulated seawater. The sample to be tested is released into the top of the test section and it falls through the test section and collects in a pan located at the base of the column. The catch pan is supported on load cells that measure the time history of weight accumulation in the pan.

Figure 4-2. Fall Velocity Test Rig (FVTR).
The sample to be tested is released into the top of the FVTR test section. The material settles through the test section and is collected in a catch pan at the bottom. The pan hangs on two load cells that are used to determine the time history of mass accumulation in the catch pan.

The test section is composed of several sections of 12-in. O.D. (11.5-in. ID) acrylic tubes that are joined with flanges to create an approximately 15-foot vertical column of water through which a sample falls. The test section is attached to a 16 in. x 12 in. reducing tee at the base that houses the sample catch pan. The ends of the tee are covered with clear acrylic flanges so that the catch pan area can be visually monitored during a test.

The FVTR uses simulated seawater as the test fluid. The seawater test fluid is prepared in a holding tank, which also serves to store the test fluid when the column is drained between experimental runs. The seawater test fluid is made by adding Instant Ocean brand aquarium salt to deionized water. For the present testing, the test fluid had a specific gravity of 1.022. The test section is filled by pumping the test fluid from the tank into the FVTR. When it is necessary to remove and clean the catch pan, the test fluid is pumped from the test section back into the storage tank. The system piping is designed so that the test fluid is filtered as it both enters and exits the test section.

When SBM droplets reach the bottom of the test section, they are captured in a stainless steel catch pan. The catch pan has a slightly larger diameter than the test section and is located directly beneath the lower end of the test section, as shown in the lower right-hand photograph in Figure 4-2. The catch pan is positioned so that there is only about a 1/4-in. gap between the end of the test section and the top edge of the pan. Due to the volume of material that could be contained in the catch pan, it was possible to run a number of experiments before the column had to be drained and the pan removed for cleaning.

4.2.1 Weight Measurement Instrumentation

To determine fall velocity distributions, it is necessary to measure the time history of the mass accumulation in the catch pan. This is done by suspending the catch pan from two load cells that measure the weight of the pan and its contents. As shown in Figure 4-2, the load cells are located above the top of the test section and are connected via long cables to a platform in the base that supports the catch pan. Each of the platform support cables is located inside of a 2-in. clear PVC tube that is connected to the base of the FVTR. These tubes are located on either side of the main 12-in. tube and they extend above the top of the test section. Because the water level in the 2-in. tubes will be the same as it is in the test section, this arrangement makes it possible to run the support cables between the platform and the load cells without using seals that would contact the cables and interfere with the measurements. A clear material was chosen for the tubes so that it would be possible to verify that the support cables are centered and not contacting the inside walls of the tube. To prevent overloading and damaging the load cells during column draining (when the catch pan remained full of sample material and water), the load cells were removed from the system and replaced with rigid links.

The load cells used in the FVTR were Interface, Inc. Model SMT1-5.6 sensors with a 5.6-lbf capacity. Each load cell was connected to an Interface, Inc. Model SGA strain gauge transducer amplifier that produced a 0-10 VDC signal proportional to the applied load. A full calibration was performed on each load cell prior to its first use and the sensors were periodically checked during the testing to verify their operation. The stated catalog accuracy for these load cells is ±0.05% of full scale for nonlinearity and ±0.03% of full scale for hysteresis.

The signals from the load cells were read using an HP 34970A datalogger. A computer connected to the datalogger was used for data visualization and storage. In a few of the initial experiments, data from both load cells were recorded at one-second intervals, but for the majority of the testing, a one-half-second sampling time was used. The datalogger was calibrated prior to the start of this testing.

4.2.2 Sample Release Methods

Three different methods were used for introducing test samples into the FVTR. For the FVTR verification tests (discussed below), a mixing chamber was used in which the silica particles were combined with water prior to dumping the whole mixture into the test section. The overboard spill experiments were done by simply pouring the SBM sample by hand into the test section from a container positioned a few inches above the surface of the water. A specialized piston and cylinder apparatus was used for the submerged jet experiments.

The silica samples used in the FVTR verification tests were released into the test section using a mixing chamber located at the top of the column as shown in Figure 4-3. This method was used to maintain consistency with the procedures employed in previous FVTR verification tests so that the resulting test data could be compared with historical data for the FVTR. The mixing chamber is a container constructed of 6-in. PVC pipe that is attached to the top of the test section with a hinge. Water is pumped into the bottom of the mixing chamber through two ports. Water flowing from these ports creates jets inside the chamber that mix and rotate the sample and help to break it apart prior to introducing the sample into the column. After about one gallon

of seawater is forced into the mixing chamber, the chamber is upended to dump the sample/water mixture into the test section. After dumping, the flow from the jets is continued for about 2-3 seconds to wash out any material that remains in the chamber.
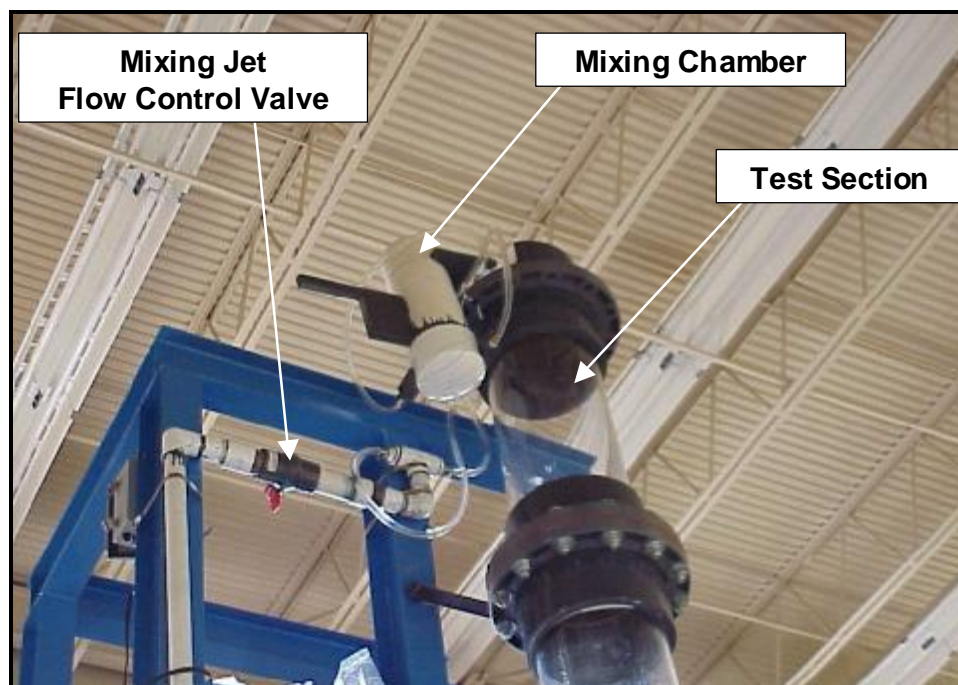
Figure 4-3. FVTR Sample Mixing Chamber.
This sample mixing chamber was only used to perform the facility verification tests. It was not used for the SBM tests.

The submerged jet experiments were performed by forcing the SBM sample out of a nozzle using the sample injection device shown in Figure 4-4. The sample injector consisted of a piston and cylinder connected to a nozzle. The SBM sample to be tested was loaded into the cylinder below the piston and air pressure was applied on top of the piston creating a jet as the mud was forced out through the nozzle. By changing the air pressure, different jet velocities could be achieved. The flow from the jet was switched on and off by a 3/8-in. ball valve located at the cylinder outlet. The nozzle was fabricated from 1/4-in. nominal OD stainless steel tubing that was cut on a lathe to form a square end with a 0.455-cm ID. A pressure transducer was connected to the air inlet of the injector so that the pressure applied before and during the injection process could be monitored.

Once filled, the injector was mounted on a flange at the top of the test section so that the nozzle was positioned several inches below the surface of the water. The nozzle was oriented horizontally and located against one side of the test section tube so that the resulting jet sprayed across the diameter of the test section. To perform an experiment, the cylinder was filled with the SBM sample and weighed and the injector was placed into position at the top of the test section. The selected air pressure for the experiment was applied to the injector and allowed to stabilize. The actual injection was performed by opening and closing the injection valve by hand and timing the duration of flow with a stopwatch. At the conclusion of a test, the injector was removed and weighed again. Knowledge of the change in injector mass and the elapsed time of injection was used to determine the jet velocity.
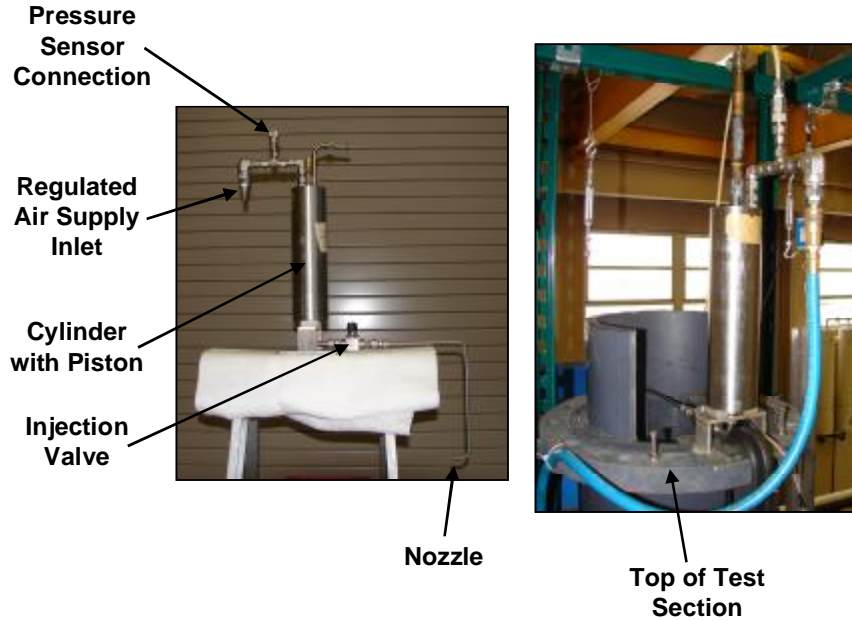
Figure 4-4. Sample Injector for Submerged Jet Experiments.
The photo on the left shows the injector itself and the photo on the right shows the injector mounted in position at the top of the FVTR test section. By varying the air pressure supplied to the injector, different jet velocities could be achieved.

4.2.3 FVTR Data Analysis

The data collected from the experiments are simply a time history of the readings from each individual load cell, so after a test is complete, the data recorded during the experiment must be processed to determine fall velocity distributions. The data analysis procedure begins with a summation of the individual load cell weight measurements (W_{LC1} and W_{LC2}) corresponding to each discrete data scan:

$$W_i = W_{LC1,i} + W_{LC2,i}$$

where *i* represents the time of an individual data scan. The result is a time history of the weight accumulation in the catch pan. The next step is to subtract the tare weight (W_0) from each reading to obtain the net weight accumulation in the pan due to the SBM droplets only:

$$W_{net,i} = W_i - W_0$$

Because the load cells measure the weight of the pan and its contents in the seawater, the effects of buoyancy must be taken into account when analyzing the test data. Thus, the conversion of the actual measured weight of the catch pan contents to the weight the material would have in air (W^{air}) is given by:

$$W_{net,i}^{air} = \frac{W_{net,i}}{\left(1 - \dfrac{g_{fluid}}{g_{sample}}\right)}$$

where γ_{fluid} is the specific gravity of the seawater and γ_{sample} is the SBM sample specific gravity.

The fall velocity corresponding to each of the discrete times (t_i) in the dataset is defined as the velocity a droplet would have to fall from the top of the column to the bottom of the catch pan in that time. Thus, each data scan time (t_i) will correspond to a certain fall velocity ($V_{fall,i}$) given by:

$$V_{fall,i} = \frac{L}{t_i}$$

where L is the distance through which the material fell before reaching the catch pan. Also, at the same discrete time, the fraction of the total sample mass in the pan, or cumulative weight fraction (WF_i) is given by:

$$WF_i = \frac{W_{net,i}^{air}}{W_{tot}}$$

where W_{tot} is the weight of the sample introduced into the FVTR as determined by weighing of the sample material prior to testing.

With these quantities calculated, the test results can be expressed graphically in plots that show fall velocity ($V_{fall,i}$) as a function of cumulative weight or mass fraction (WF_i). If all of the sample material is collected in the catch pan and the specific gravities are determined accurately, the final mass fraction should be very close to 1.0, meaning that the final weight in the pan is equal to the starting weight.

It should be noted that the fall velocity results are affected by how the test start time and particle fall distance is defined. The starting time for each test was taken to be the time at which the material entered the water of the FVTR. Since the fluid height in the column changes after a sample is introduced into the column, the depth of the fluid is not the same at the beginning and end of an experiment. For all of the present testing, the fall distance was defined as the distance from the bottom of the catch pan to the top surface of the fluid in the column prior to introducing the test sample. It was felt that this choice better reflected the amount of fluid that all of the material fell through (as opposed to using the final fluid level). For the submerged jet experiments, the distance between the nozzle and the pan was always the same. When consecutive experiments were performed without cleaning the catch pan, no correction to the fall distance was made for the buildup of material in the bottom of the pan, as it was not possible to accurately determine the thickness of this layer. However, in all cases, the thickness of this layer of material was small compared to the total fall distance.

4.2.4   FVTR Verification Tests

Prior to beginning the SBM fall velocity experiments, the FVTR and data acquisition system operations were verified by measuring the fall velocity of a well-characterized sample of unground silica particles. The material used was #1 Q-ROK supplied by U.S. Silica. The verification tests were performed using procedures and material identical to that used in a number of previous facility qualification tests so that direct performance comparisons to historical data could be made. The specific gravity of these particles is stated by the

manufacturer to be 2.65. This value was confirmed by laboratory measurement. The particle size distribution for the #1 Q-ROK is given in Table 4-1.

Table 4-1. Size Distribution for #1 Q-ROK.
Particle size distribution as determined by the vendor for the material used in the qualification tests.

USA STD SIEVE	SIEVE OPENING (millimeters)	FRACTION RETAINED (%)	CUMULATIVE RETAINED (%)
20	0.850	0.005	0.005
30	0.600	0.095	0.100
40	0.425	0.400	0.500
50	0.300	0.350	0.850
70	0.212	0.140	0.990
100	0.150	0.008	0.998
140	0.106	0.001	0.999
200	0.075	0.001	1.000

The fall velocity results as a function of sample mass fraction for two qualification tests conducted with the #1 Q-ROK are shown in Figure 4-5, along with some of the previous results and a theoretical fall velocity prediction. The theoretical fall velocity prediction is based on the particle size distribution provided by the vendor and was computed using drag coefficients given by Perry and Green.[20] In this analysis, it has been assumed that the particles are spherical and do not interact with each other as they fall. The new data taken for this project are plotted with the red and blue symbols. The previous experimental data are plotted using black symbols. As can be seen, the fall velocity results obtained from the two most recent qualification runs are quite consistent with each other and they agree closely with previous tests and the theoretical prediction.
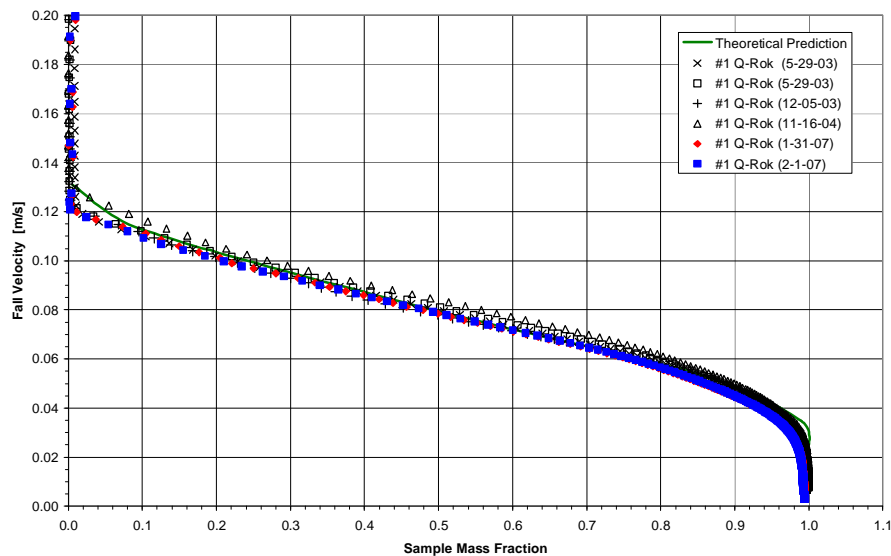
Figure 4-5. Fall Velocity for Two Qualification Test Runs with #1 Q-ROK Compared with Past Tests and the Theoretical Prediction.
Data from the FVTR verification tests done for this project are shown with the colored symbols. The fall velocity obtained from the latest run is consistent with the previous test runs and the theoretical fall velocity curve for these particles.

The final sample weight in the catch pan at the end of the experiment (corrected for buoyancy) was 0.5% less than the #1 Q-ROK sample weight as measured with an electronic scale prior to the test for one case and 0.6% less for the other. In both tests, it was observed that some of the #1 Q-ROK remained in the mixing chamber and did not get introduced into the column. This small residual amount likely accounts for the mass balance discrepancy. From these verification tests, it was concluded that the FVTR was performing satisfactorily and was ready for use in the SBM fall velocity tests.

4.3   SBM SAMPLES

SBM samples for use in the fall velocity testing were obtained from three of the major suppliers for GOM drilling operations: Halliburton, Baker-Hughes, and MI Swaco. Two of the companies provided two samples each with different densities. All of the samples were IO SBMs typical of what is used in the GOM. The samples from Halliburton were used muds that had been cleaned and recycled. It is not known if the other samples were new or recycled.

These mud samples were stored for a period of several months prior to being used in the testing. When the containers were first opened, the various fluids in the mud samples were somewhat separated. To make sure that the samples were well blended prior to use, they were mixed for one-half to one hour with a mechanical stirrer. After this period of time, the samples appeared to be homogeneous. This process was repeated prior to each use of a sample.

Because it was not the purpose of this investigation to draw any conclusions about the performance of one SBM formulation versus another, the five individual samples will be identified in this report using a generic naming system: Mud A, Mud B, Mud C, Mud D, and Mud E. This system has been used to prevent the test results from being linked to a specific mud.

The densities and corresponding specific gravities for each SBM sample are given in Table 4-2. The densities were determined by using an electronic scale to measure the net mass of the sample contained in a mud cup of known volume. The densities were verified by using a mud balance. All measurements were made with the mud at room temperature.

Table 4-2. Densities of the SBM Samples.
The density of each sample was measured prior to using it in the experiments.

MUD SAMPLE	DENSITY (lb/gal)	SPECIFIC GRAVITY
A	12.11	1.45
B	14.83	1.78
C	13.56	1.63
D	11.70	1.40
E	9.76	1.17

The rheological properties for each mud were estimated by testing a sample of the mud in a Fann rotational viscometer. Shear stress was measured at six different rotational speeds (shear rates) and the results were analyzed to determine the plastic viscosity, PV, and yield point, YP,

terms in the non-Newtonian Bingham plastic fluid model. The Bingham model is the most commonly used non-Newtonian fluid model for drilling fluids and it relates the fluid shear stress, τ, to the shear rate, γ, with the following equation:

$$t = YP + PV(g)$$

Details on this fluid model and the use of a rotational viscometer to determine the Bingham Plastic model constants can be found in most references on drilling fluids. As with the density, all measurements were made at room temperature. The results of the rheological measurements are given in Table 4-3.

Table 4-3. Rheological Properties of the SBM Samples.

These properties were measured by testing each sample in a Fann Rotational Viscometer.

MUD SAMPLE	VISCOMETER SPEED (rpm)	VISCOMETER READING	PV (cP)	YP (lb/100ft^2)
A	600	93	44	5
	300	49		
	200	34		
	100	19		
	6	3.5		
	3	2.5		
B	600	173	79	15
	300	94		
	200	67		
	100	37		
	6	8		
	3	6		
C	600	119	53.5	12
	300	65.5		
	200	47		
	100	32		
	6	7.5		
	3	6		
D	600	125	55	15
	300	70		
	200	50.5		
	100	29.5		
	6	8.5		
	3	8		
E	600	144	60	24
	300	84		
	200	61		
	100	36.5		
	6	9		
	3	8		

4.4 OVERBOARD SPILL TEST RESULTS

The muds were tested for the overboard spill case by pouring each one into the top of the FVTR test section from a container held a few inches above the surface of the water. As soon as the SBM entered the water, it would break up into droplets. By visual observation, it was not possible to tell if the droplets were breaking into smaller droplets or changing size as they fell. Figure 4-6 is an image taken from the video recording of one test showing the leading edge of the droplets as they neared the bottom of the test section. Although the sample was poured into the center of the test section, by the time the droplets reached the bottom they had spread out fairly uniformly over most of the tube cross-section.

Figure 4-6. Photograph Taken Near the Bottom of the Test Section Showing the Arrival of the Leading Edge of the SBM Droplets.
By the time the SBM reaches the bottom of the test section, it has broken into small droplets.

The test conditions for each of the overboard spill experiments are summarized in Table 4-4. One fall velocity test was performed with each of the mud samples, except for Mud B, which was tested three separate times to assess the repeatability of the results. For each fall velocity experiment, this table shows the mud tested, the specific gravity of the mud, and a comparison of sample material mass measured before and after the test. The initial sample mass represents the amount of mud released into the test section, and the recovered mass is the total amount of sample material accumulated in the catch pan at the end of a test (corrected for buoyancy to give the mass in air). The criteria used for determining the end of a test was to verify that no falling droplets were visible in the test section and that the weight of the catch pan had essentially stabilized. The small differences in the mass balance show that the experiments were run long enough to allow practically all of the sample material to settle. For these experiments, the duration of a test was typically between 15 and 20 minutes. Although not shown in this table, all of the tests were performed with the mud samples and the seawater test fluid at room temperature (65°F-75°F). The same test fluid was used for all of the experiments, and it had a specific gravity of 1.022, as determined by hydrometer measurement.
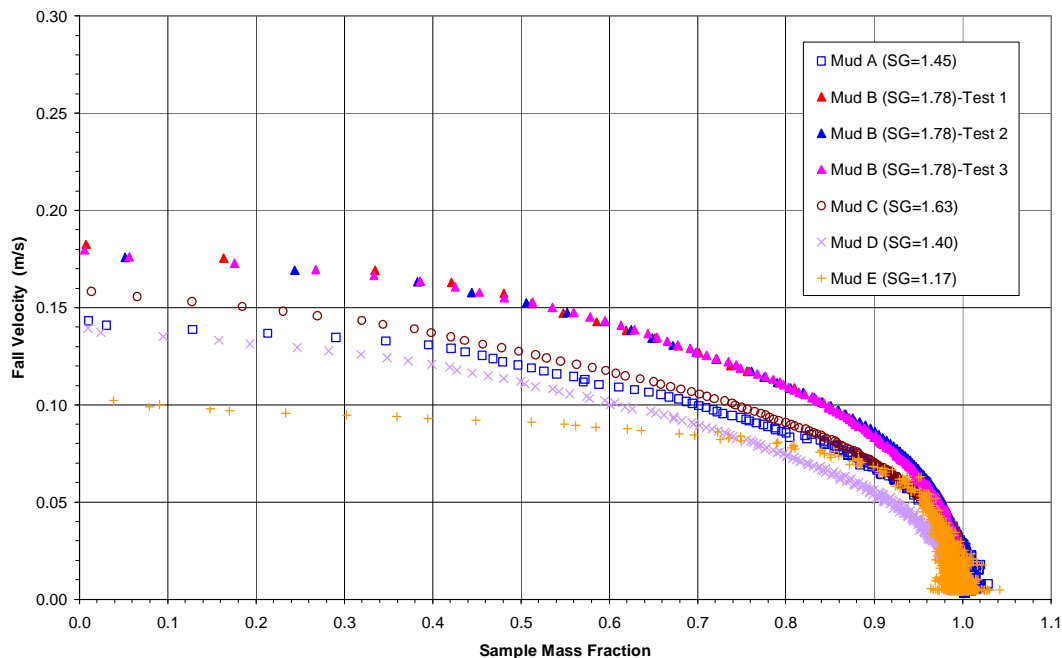
Figure 4-7 shows the fall velocity distribution for each of the SBM samples as a function of mass fraction for the overboard spill case. The general shape of the distributions is the same

for all of the samples, with the possible exception of Mud E. The majority of the sample masses fell with a velocity between 0.05 m/s and 0.20 m/s. Differences in the fall velocity between samples are due to the sample specific gravities. In fact, the order of curves from highest to lowest fall velocity (B, C, A, D, E) exactly matches the ordering of the sample specific gravities. Mud B was tested three separate times and the results show that the resulting fall velocity distribution is very repeatable.

Table 4-4. Conditions for the Overboard Spill Fall Velocity Tests.
One test was performed on each mud sample, except for Mud B, which was tested multiple times to investigate the repeatability of the fall velocity results.

MUD SAMPLE	SPECIFIC GRAVITY	INITIAL SAMPLE MASS (g)	RECOVERED MASS (g)	DIFFERENCE IN MASS
A	1.45	566.9	573.9	+1.2%
B (Test 1)	1.78	685.3	688.1	+0.4%
B (Test 2)	1.78	640.1	641.6	+0.2%
B (Test 3)	1.78	651.8	651.0	-0.1%
C	1.63	627.8	627.7	0.0%
D	1.40	543.5	541.0	-0.5%
E	1.17	243.3	245.0	+0.7%

Figure 4-7. Fall Velocity Distributions for the Overboard Spill Case.
All of the muds have similarly-shaped fall velocity distributions, but the actual fall velocities are not the same due to differences in the sample specific gravities.

In processing the data for the fall velocity distribution plot, a cutoff was applied in which fall velocity results were not calculated until the catch pan mass had increased by at least 1.0 g (0.5 g in some cases). Before the leading edge of the SBM droplets reaches the catch pan, vibrations of the FVTR structure and other disturbances cause slight fluctuations in the load cell

readings (typically less than 1.0 g). These fluctuations appear as a change in the net catch pan weight and, thus, get recorded as fall velocity data points. To eliminate this problem, this cutoff was implemented to ensure that the catch pan weight was increasing due to actual sample accumulation.

These same fluctuations also cause the scatter seen in the fall velocity data at mass factions near 1.0. In this case, most of the sample is already in the catch pan and the weight is only slowly increasing as the smallest, lightest droplets settle into the pan. The random fluctuations in the load cell readings then get recorded as a change in sample mass fraction. The scatter is particularly noticeable for the lower specific gravity samples (such as Muds D and E) in which the total net weight of the sample in the seawater is small due to buoyancy. For these samples, a small variation in load cell reading can amount to a few percent of the total sample mass.

4.5   SUBMERGED JET TEST RESULTS

The submerged jet tests were performed by introducing the SBM sample into the FVTR test section using the injection apparatus described in subsection 4.2.2. Each SBM sample was tested at four jet velocities, with the exception of Mud E. There was only enough of the Mud E sample to perform three tests. The test conditions for the submerged jet experiments are summarized in Table 4-5. The mass flowrate shown in this table was computed from the mass injected (as determined by weighing the injector before and after releasing a sample) and the injection duration. As was done for the overboard spill experiments, a comparison was made between the injected mass and the mass recovered in the catch pan. The somewhat larger differences in the mass balance for these experiments are most likely due to mud sticking to the walls of the test section and difficulties in measuring the small amount of mass injected in some of the tests. The jet velocity was computed from the mass flowrate using the jet area (0.455-cm diameter, 0.162-cm^2 area) and the density of the sample. The Reynolds number and Ohnesorge numbers were calculated using the equations shown in subsection 3.2. In computing these two dimensionless numbers, the viscosity was assumed to be equal to the PV value for the sample (see Table 4-3) and the interfacial tension was taken to be 25 dyne/cm. The duration of these experiments varied from a few minutes to about one hour. For the low jet velocities, the mud fell in large droplets and the tests were essentially over within a few minutes. At higher jet velocities, small droplets were formed that required up to one hour to settle through the test section. Although not shown in this table, all of the tests were performed with the mud samples and the seawater test fluid at room temperature (65°F-75°F). The same test fluid was used for all of the experiments, and it had a specific gravity of 1.022, as determined by hydrometer measurement.

To make the submerged jet tests applicable to as wide a range of conditions as possible, it was necessary to choose test conditions that produced jets representative of all three jet flow regimes (Rayleigh breakup, transition, and atomization). In Figure 4-8, the test conditions (in terms of Reynolds number and Ohnesorge number) for the submerged jet tests have been plotted on Figure 3-7 to show the expected jet regimes for each test. Although the regime boundaries in this figure were developed from experiments done with crude oil, this data can be used as a guideline to estimate the type of jet breakup that would be expected for the SBM tests. From this figure, it appears that the velocities used for the submerged jet tests should be sufficient to give a range of test points that spans across all three jet flow regimes.

Table 4-5. Conditions for the Submerged Jet Fall Velocity Tests.

Each mud was tested at four different jet velocities, with the exception of Mud E. In all tests, the jet diameter was 0.455 cm and the interfacial tension was taken to be 25 dyne/cm.

| TEST NO.	MUD SAMPLE	MASS INJECTED (g)	RECOVERED MASS (g)	DIFFERENCE IN MASS	INJECTION DURATION (s)	MASS FLOWRATE (g/s)	DENSITY (g/cm^3)	VISCOSITY (cP)	JET VELOCITY (cm/s)	REYNOLDS NUMBER	OHNESORGE NUMBER
1	A	43.7	45.3	+3.8%	5.9	7.4	1.45	44	31	47	0.108
2	A	191.4	197.5	+3.2%	6.4	29.9	1.45	44	127	190	0.108
3	A	471.1	475.3	+0.9%	5.8	81.2	1.45	44	345	517	0.108
4	A	634.2	634.2	0.0%	5.1	124.4	1.45	44	528	791	0.108
5	B	32.8	31.1	-5.2%	5.9	5.6	1.78	79	19	20	0.176
6	B	139.1	139.7	+0.4%	5.6	24.8	1.78	79	86	88	0.176
7	B	309.3[a]	309.3	0.0%[a]	5.5	56.2	1.78	79	195	199	0.176
8	B	506.7	486.9	-3.9%	5.5	92.1	1.78	79	319	327	0.176
9	C	42.5	41.3	-2.8%	5.6	7.6	1.63	54	29	40	0.124
10	C	176.7	178.1	+0.8%	5.5	32.1	1.63	54	122	168	0.124
11	C	391.5	387.8	-0.9%	5.1	76.8	1.63	54	291	402	0.124
12	C	659.8	625.6	-5.2%	5.5	120.0	1.63	54	455	628	0.124
13	D	24.9	24.9	0.0%	5.5	4.5	1.40	55	20	23	0.138
14	D	126.3	128.7	+1.9%	5.6	22.6	1.40	55	99	115	0.138
15	D	335.7	336.2	+0.1%	5.3	63.3	1.40	55	278	323	0.138
16	D	512.4	491.6	-4.1%	5.1	100.5	1.40	55	441	512	0.138
17	E	112.8	118.1	+4.7%	5.5	20.5	1.17	60	108	96	0.165
18	E	322.3	331.3	+2.8%	5.9	54.6	1.17	60	288	255	0.165

[a]The injector was not weighed following this test, so the net mass injected could not be determined. For this test, the mass injected was assumed to be equal to the recovered mass.
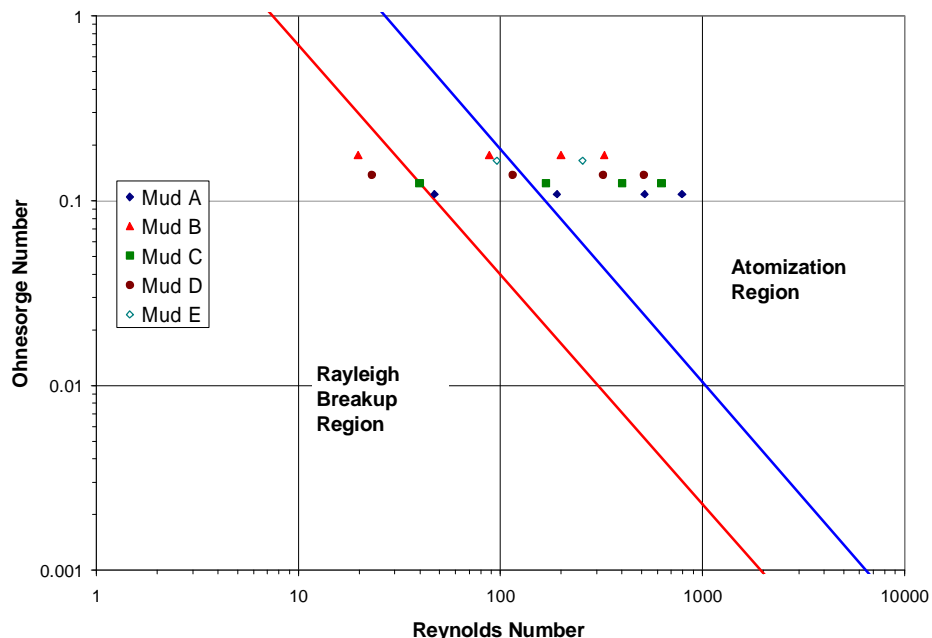
Figure 4-8. Experimental Test Points Plotted on Figure 3-7 Showing the Jet Breakup Regimes.
The jet velocities in the experiments gave a range of test points that spanned across the different breakup regimes.

The velocities needed to create jets in each breakup regime were confirmed with a series of benchtop experiments in which SBM jets were visualized in a rectangular tank. Still images taken from the video recordings of each of the flow visualization tests are shown in Figure 4-9. At the lowest velocity, the jet flows smoothly out of the nozzle and then begins to break up at some distance downstream forming large drops. The jet in the transitional regime looks similar to the low-velocity jet, except that a short distance from the nozzle tip there are noticeable waves forming at the jet/water interface. At the highest velocity, the jet breaks into a spray of small droplets. No attempt was made to exhaustively verify the regime boundaries given by Masutani and Adams.[14] Rather, the purpose of these experiments was to verify that the test conditions had been chosen properly to give jets that spanned across the different breakup regimes. The jet regimes were also verified during the individual SBM fall velocity experiments.

Figure 4-10 through Figure 4-14 show the fall velocity distributions for each of the SBM samples as a function of mass fraction for the submerged jet case. The individual curves on each plot represent a fall velocity test conducted for a specified jet condition. The jet velocity and Reynolds number are shown in the figure legends, and more detailed information about the test conditions can be found by using the test number and referring to Table 4-5. For comparison, the fall velocity distribution obtained from the overboard spill experiment has been plotted, along with the submerged jet results for each mud sample. The overboard spill results are shown with open symbols. In processing the data for these plots, the same low-weight cutoff, as described in subsection 4.4, was applied. The fluctuations in fall velocity distributions at mass factions near 1.0 that were discussed in that subsection are also seen in some of the submerged jet test results. In this case, the fluctuations are due to the lower sample specific gravities and the small total amount of mass injected at low jet velocities.
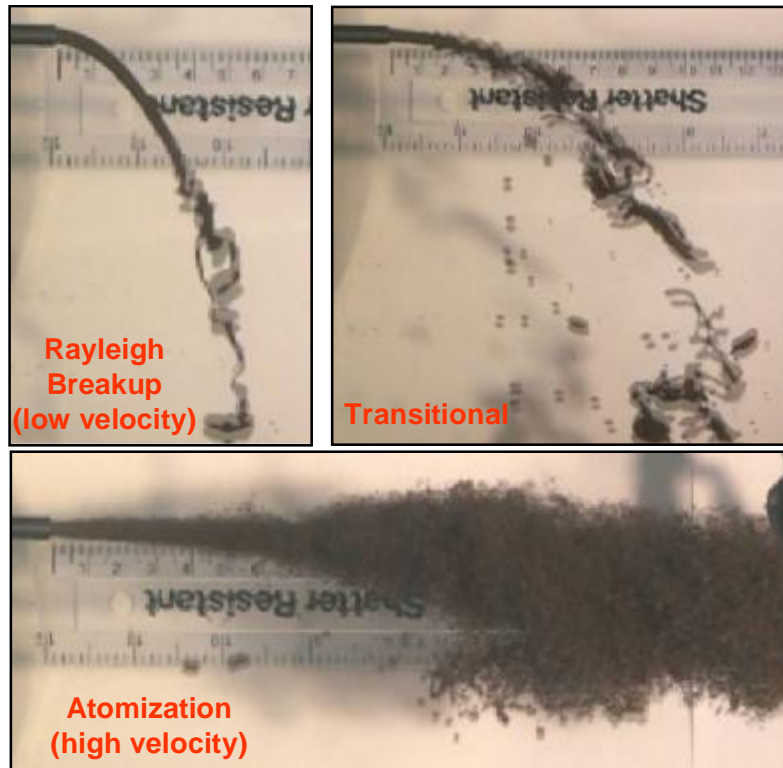
Figure 4-9. The Three Jet Breakup Regimes for an SBM Jet.
These tests confirmed that the range of experimental conditions was sufficient to produce jets typical of all three breakup regimes.

Comparison of the curves for the different jet conditions shows that, for the same SBM, increasing the jet velocity leads to droplets with a lower fall velocity. The highest fall velocities were for jets in the Rayleigh breakup and transition regimes. In these regimes, the SBM tended to flow smoothly out of the nozzle and break up into large drops that fell very rapidly (see Figure 4-9). As the jet velocity increased, the resulting atomization created smaller drops that took longer to fall. For example, for Mud A, the fall velocity distribution for the 31 cm/s jet is almost flat, indicating that most all of the sample mass settled with the same fall velocity (approximately 0.12 m/s). At the next highest jet velocity (127 cm/s), the fall velocity distribution follows the 31 cm/s jet results up to a mass fraction of about 0.8, where it begins to curve downward. The separation of these two curves is due to the presence of smaller, more slowly falling drops formed in the 127 cm/s jet. As the jet velocity is increased to 345 cm/s, the resulting droplets have fall velocities much lower than those obtained for the 31 cm/s and 127 cm/s jets. In addition, the shape of the fall velocity distribution is noticeably different from the distributions in the lower velocity jet cases. The overall lower fall velocity shows that the higher jet velocity has produced smaller, more slowly falling droplets and the shape suggests that there has also been a change in the distribution of drop sizes. These results are consistent with the expected behavior of jets in the atomization regime. Although the shape remains similar to the 345 cm/s jet, even lower fall velocities are obtained for the highest velocity jet (528 cm/s). Similar trends in the relationship between fall velocity and jet velocity were seen in the other SBMs tested.

Comparison of the fall velocity distributions from the overboard spill and submerged jet experiments shows that fall velocities for the two cases are within the same range for the samples

tested. However, the shape of the overboard spill fall velocity distribution is distinct from the jet results, suggesting that the process of pouring the sample into the water results in a drop size distribution that differs from that produced by a jet. It is also interesting to note that a portion of overboard spill fall velocity distributions typically has slightly higher fall velocities than the jet cases. One reason for the higher fall velocities in the overboard spill experiments (as compared to the jet cases) may be the initial downward momentum of the fluid that results from it entering the test section from above, as opposed to the jets, which entered horizontally.
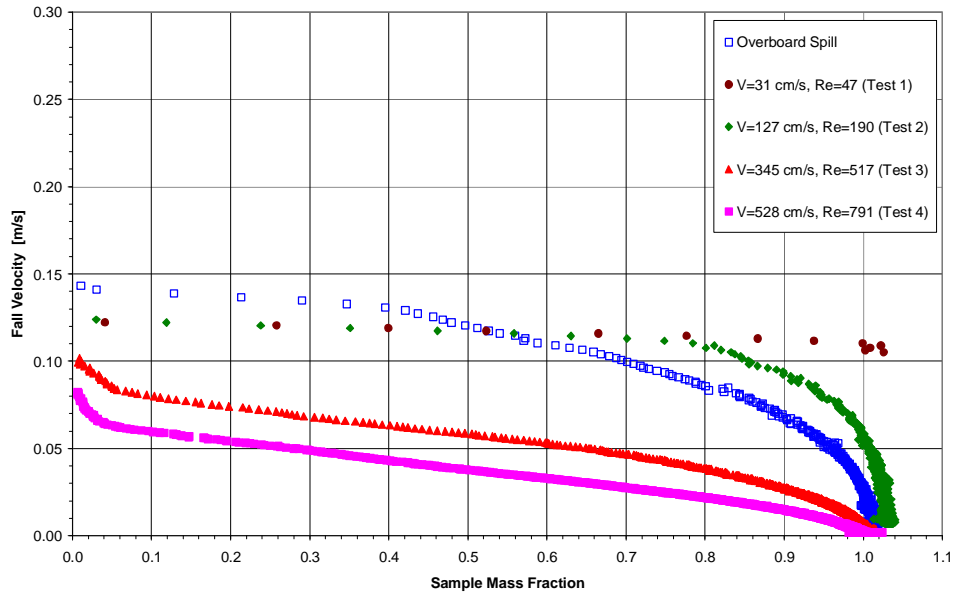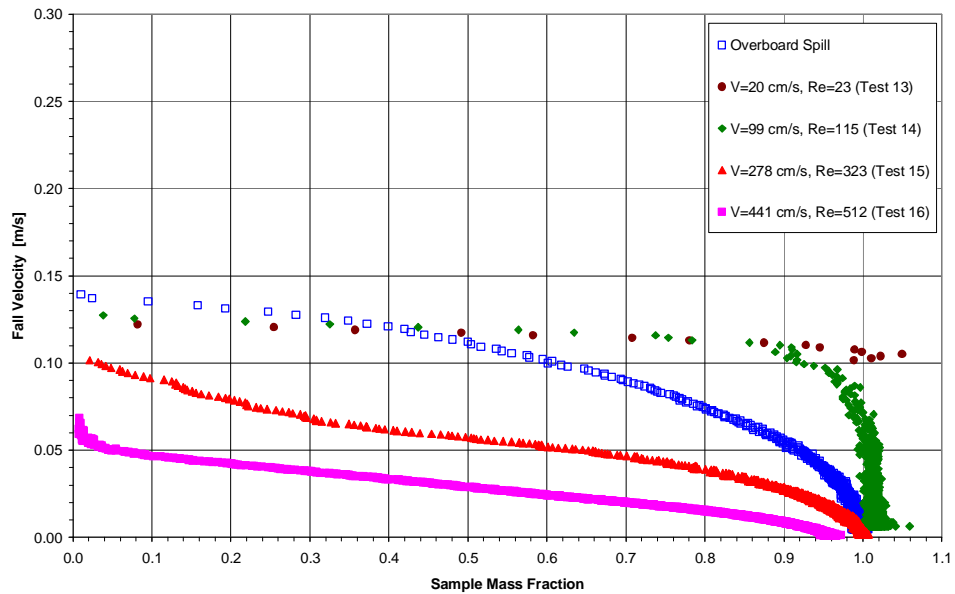

Figure 4-10. Fall Velocity Distributions for the Submerged Jet Case for Mud A.
The jet velocity and Reynolds number for each curve is this figure is shown in the figure legend. As the jet velocity increases, smaller drops with a lower fall velocity are formed.
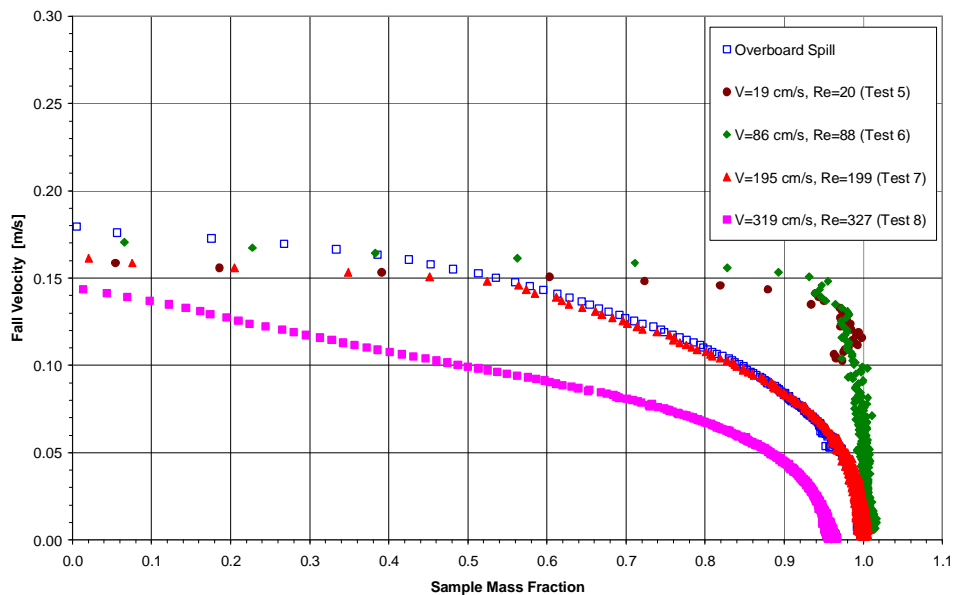
Figure 4-11. Fall Velocity Distributions for the Submerged Jet Case for Mud B.
The jet velocity and Reynolds number for each curve is this figure is shown in the figure legend. As the jet velocity increases, smaller drops with a lower fall velocity are formed.
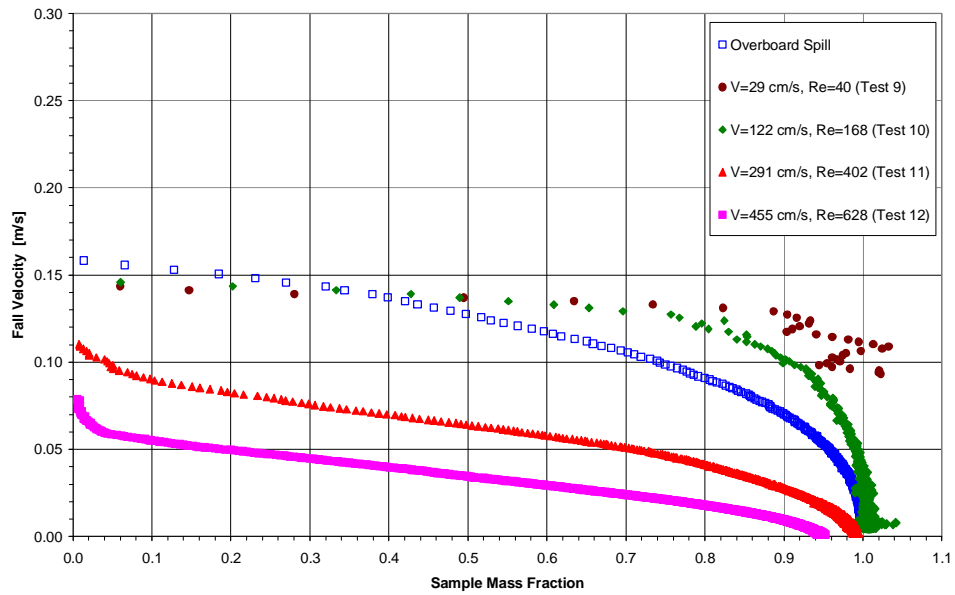
Figure 4-12. Fall Velocity Distributions for the Submerged Jet Case for Mud C.
The jet velocity and Reynolds number for each curve is this figure is shown in the figure legend. As the jet velocity increases, smaller drops with a lower fall velocity are formed.

Figure 4-13. Fall Velocity Distributions for the Submerged Jet Case for Mud D.
The jet velocity and Reynolds number for each curve is this figure is shown in the figure legend. As the jet velocity increases, smaller drops with a lower fall velocity are formed.

Figure 4-14. Fall Velocity Distributions for the Submerged Jet Case for Mud E.
The jet velocity and Reynolds number for each curve is this figure is shown in the figure legend. As the jet velocity inc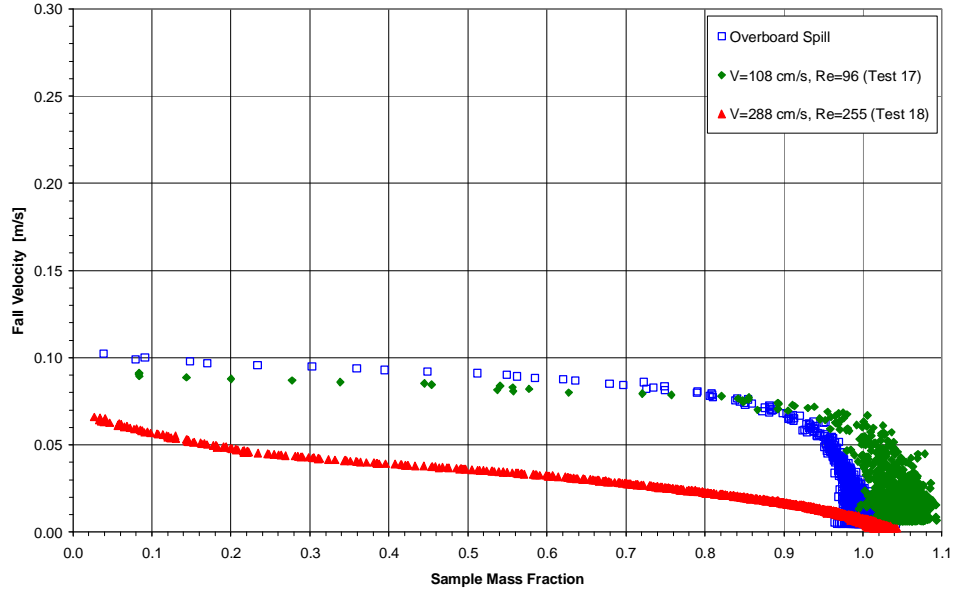reases, smaller drops with a lower fall velocity are formed. A full set of test cases could not be completed with this mud as there was not a sufficient amount of sample material.

5. CONCLUSIONS

The purpose of this project was to characterize the fall velocity distributions that would result from an accidental release of synthetic-based muds (SBMs) in offshore waters. The investigation focused on determining how fall velocity distributions for SBMs used in Gulf of Mexico operations are affected by release conditions. It is expected that the present work will contribute to the understanding of how SBM spills disperse in the marine environment and this understanding will be important in assessing the impact of spills on the marine environment surrounding drilling and production platforms and in developing mitigation strategies for spills.

The project included an industry operations survey that was performed in order to gain a better understanding of the operational conditions and characteristics of incidents involving the discharge of SBMs in the Gulf of Mexico (GOM). The results of the survey showed that Internal Olefin (IO) SBMs with densities in the range of 9-15 lb/gal were the most commonly used muds in the GOM. In general, SBM spills can be considered to come from two generic sources: a discharge of fluid overboard and subsea releases. From a review of reported spill data, it was determined that about equal amounts of spilled fluid can be attributed to these two sources. However, viewing the data in terms of the number of occurrences of each type reveals that overboard spills occur much more frequently than other types and these are most often caused by human error. Based on the information gained from the operations survey, it was concluded that two general cases (overboard spill and submerged jet) could be considered to be representative of the majority of GOM SBM spills.

Although the focus of this project is on fall velocity, a literature review and a limited modeling effort was performed to identify existing fluid breakup models from published literature and use the models to predict SBM drop size for different SBM release conditions. Understanding fluid breakup mechanisms provides considerable insight into how release conditions affect the resulting fall velocity distributions and how SBM behaves once it enters the seawater. Little technical literature was found that was directly applicable to predicting the drop sizes formed when an SBM (a non-Newtonian fluid) is released into seawater. For the case of mud drop breakup under buoyant flow conditions, methods to estimate the maximum stable drop size were found for Newtonian fluids, but not for non-Newtonian fluids. For the case of droplet formation in high-velocity jets, correlations were identified that predict three jet breakup regimes (Rayleigh, transition, and atomization). One key characteristic of these regimes is that Rayleigh breakup tends to form drops of a uniform size, while atomization produces a distribution of drop sizes. Most of the experimental data and modeling work that were found related to laminar jet breakup, or Rayleigh breakup. In this jet breakup regime, the drop size formed is typically on the order of the jet diameter and the drop size is independent of the jet velocity. Very little information was found on the drop sizes produced from higher velocity jets that cause fluid atomization. The correlations that were found were used to make estimates of the distribution of expected drop sizes.

The experimental work was performed using the SwRI Fall Velocity Test Rig (FVTR). The FVTR is a 15-ft tall water-filled settling column in which a sample to be tested falls through the column and collects in a pan at the bottom. The time history of the weight accumulation in the catch pan can be postprocessed to determine fall velocity as a function of the sample mass

fraction. Two series of fall velocity tests were performed to represent the two general spill cases identified from the operations survey. In the first series of tests, intended to represent an overboard spill, SBM was poured from a container into seawater in the FVTR test section. The case of an underwater release from a pressurized source was simulated by discharging SBM from a submerged jet into the FVTR test section. For both spill scenarios, experiments were performed with five different IO SBMs typical of those used in GOM drilling operations. For all of the muds tested in the overboard spill experiments, similar fall velocity distributions were measured, but the magnitude of the fall velocity depended on the SBM specific gravity. For the submerged jet case, each mud was tested at several jet velocities in order to achieve a range of conditions representative of the three jet breakup regimes. The fall velocity distributions obtained from the submerged jet experiments depended strongly on the jet velocity. As suggested by the information found in the published literature, as the jet velocity increased, more small droplets were formed from the breakup of the SBM jet. As the jet velocity was increased, the fall velocities moved lower due to the formation of smaller droplets. The shape of the fall velocity distributions also changed indicating that the drop size distributions were being altered at the higher jet velocities. Similar trends in the relationship between fall velocity and jet velocity were seen in all of the SBMs tested.

Based on the experience gained from this project, a few recommendations can be made for future work. These are as follows:

- One area that is not well defined is how to link the results of laboratory-scale experiments such as those described here to actual spills. Some preliminary work that was done as a part of this project (although not discussed in this report) suggests that it may not be possible to match all of the relevant dimensionless parameters between the field case and the lab experiments. Therefore, it may be beneficial to run experiments at even higher jet velocities than those used in these tests. In the present tests, the jet velocity was limited to minimize the force with which the fluid jet impacted the opposite wall of the test section tube. Performing experiments in a larger test section may be useful.

- It may also be beneficial to test some types of SBMs other than IO (or perhaps other types of drilling fluids) to determine the applicability of these results to spills of other types of fluids.

- The experimental approach from this investigation could be used as a basis for developing a standard laboratory test method for assessing drilling fluid dispersibility in seawater. With such a method, it would be possible to establish an acceptance criterion that could be used to evaluate a drilling fluid to ensure that if a spill occurred, the drilling fluid would disperse in such a way as to minimize damage to the marine environment.

6. REFERENCES

[1] Denney, D., "Seabed Effects of Synthetic-Based Drilling Mud Cuttings in the Gulf of Mexico," *Journal of Petroleum Technology*, July 2005, pp. 61-63.

[2] Bourgoyne, A., Millheim, K., Chenevert, M., and Young, F., *Applied Drilling Engineering,* SPE Textbook Series, Vol. 2, 1986.

[3] Burke, C. J. and Veil, J. A., "Synthetic-Based Drilling Fluids Have Many Environmental Pluses," *Oil and Gas Journal*, Vol. 93, n. 48, November 27, 1995, pp. 59-64.

[4] Friedheim, J. E. and Patel, A., "Technical Solutions for Environmental Problems: Novel Drilling Formulations to Minimize Environmental Impact," Proceedings of the 1999 SPE/EPA Exploration and Production Environmental Conference, SPE 52741, Austin, Texas, February 28-March 3, 1999.

[5] Veil, J. A., Burke, C. J., and Moses, D. O., "Synthetic-Based Muds Can Improve Drilling Efficiency Without Polluting," *Oil and Gas Journal*, Vol. 94, n. 10, March 4, 1996, pp. 49-54.

[6] Growcock, F. B. and Frederick, T. P., "Operational Limits of Synthetic Drilling Fluids," SPE Drilling and Completion, September 1996, pp. 132-136.

[7] Patel, A. D., "Choosing the Right Synthetic-Based Drilling Fluids: Drilling Performance Versus Environmental Impact," Proceedings of the SPE India Oil and Gas Conference and Exhibition, SPE 39508, 1998, pp. 95-108.

[8] Growcock, F. B., Andrews, S. L., and Frederick, T. P., "Physicochemical Properties of Synthetic Drilling Fluids," Drilling Conference - Proceedings, SPE 27450, 1994, pp. 181-190.

[9] U.S. Department of the Interior, Minerals Management Service, Offshore Minerals Management, OCS-Related Incidents, Significant Pollution Incidents, 2000-2006. http://www.mms.gov/incidents/SigPoll2002.htm.

[10] Grace, J. R., Wairegi, T., and Brophy, J., "Break-Up of Drops and Bubbles in Stagnant Media," *The Canadian Journal of Chemical Engineering*, Vol. 56, February 1978, pp. 3-8.

[11] Clift, R., Grace, J. R., and Weber, M. E., *Bubbles, Drops, and Particles*, Academic Press, New York, 1978.

[12] Kitamura, Y. and Takahashi T., "Stability of Jets in Liquid-Liquid Systems," *Encyclopedia of Fluid Mechanics*, Vol. 2 (N. P. Cheremisinoff, ed.), Chapter 19, Gulf Publishing Company, Houston, TX, 1986.

[13] Tang, L., Gorgas, T. J., and Masutani, S. M., "Liquid CO_2 Droplet Spectra," Proceedings of the 6th International Conference on Greenhouse Gas Control Technologies, Kyoto, Japan, October 1-4, 2002, pp. 831-836.

[14] Masutani, S. M. and Adams, E. E., "Experimental Study of Multiphase Plumes with Application to Deep Ocean Oil Spills," Final Report for U.S. Department of the Interior, Minerals Management Service, Contract No. 1435-01-98-CT-30964, 2001.

[15] Teng, H., Kinoshita, C. M., and Masutani, S. M., "Prediction of Droplet Size from the Breakup of Cylindrical Liquid Jets," *International Journal of Multiphase Flow*, Vol. 21, No. 1, 1995, pp. 129-136.

[16] Rye, H., Johansen, Ø., and Koderup, H., "Drop Size Formation from Deep Water Blowouts," Tech. Report No. STF66F98090, SINTEF, Trondheim, Norway, 1998.

[17] Johansen, Ø., "DeepBlow – a Langrangian Plume Model for Deep Water Blowouts," *Spill Science & Technology*, Vol. 6, No. 2, 2000, pp. 103-111.

[18] Reed, M. et al., "Technical Documentation for the Pipeline Oil Spill Volume Computer Model," SINTEF Report No. STF66 A03015 for the U.S. Minerals Management Service, 2003.

[19] Schroder, J. J. et al., "Liquid/Liquid Jet Dispersion," *German Chemical Engineering*, Vol. 8, 1985, pp. 248-254.

[20] Perry, R. H. and Green, D. W., *Perry's Chemical Engineers' Handbook*, Seventh Edition, McGraw-Hill, New York, 1997.